CHAPTER 5

THEORETICAL ANALYSIS AND SIMULATION

5.1 Introduction

Up to now, many computer codes and models for the fuel-coolant interaction are still being developed [40] with the different implementing methods. Sometimes, the accuracy of the models is adjusted with a set of parameters to match the result from the experiment. However, the computer code TEXAS [25] is chosen due to its availability. The code is one of the major tools used at the University of Wisconsin-Madison (UW) for the simulation of the fuel-coolant interaction during its mixing, triggering and explosion phases. TEXAS [26,41] is originally developed at Los Alamos National Laboratory as part of the SIMMER development, adapted at Sandia National Laboratories and finally modified by the UW for the simulation of the fuel-coolant interactions.

TEXAS has been tested with the high temperature fuel-coolant interaction. The prediction is more accurate and reliable in the mixing phase than in the explosion phase. Also in the explosion phase some parameters are required such as the proportional constants in the correlation for calculating the fragmentation rate, the trigger position, etc. Due to these empirical assumptions, only the mixing model of the fuel-coolant interaction will be used in this dissertation with the assumption that if the scale of the maximum pressurization from the simulation is comparable to that of the experiment, then the pressure spikes appear in the experiment is only the pressurization from mixing. If not, the pressure spikes will probably emphasize the explosion-liked interaction.

TEXAS model solves the 1-D, three-field equations. The first two fields represent the coolant vapor and the coolant liquid in an Eulerian control volume or an Eulerian cell. The last field represents the fuel in Lagrangian description within the Eulerian volume. The governing equations describing the fields in TEXAS model are briefly described in this dissertation.

5.2 Definition of Volume Fractions

In an Eulerian cell,

$$V_l + V_g = V_c \tag{5.1}$$

$$V_c + V_p = V_{cell} \tag{5.2}$$

where V_l = Coolant liquid volume

V_g = Coolant vapor volume

V_c = Coolant mixture volume

V_p = Fuel particle volume

V_{cell} = Eulerian cell volume

$$\alpha_g = \frac{V_g}{V_c} \tag{5.3}$$

$$\alpha_l = \frac{V_l}{V_c} \tag{5.4}$$

$$\alpha_f = \frac{V_p}{V_{cell}} \tag{5.5}$$

$$\rho'_g = \alpha_g \rho_g \tag{5.6}$$

$$\rho'_l = \alpha_l \rho_l \tag{5.7}$$

where α_g = Volume fractions of the vapor with respect to the coolant volume in a total volume of an Eulerian cell

α_l = Volume fractions of the liquid with respect to the coolant volume in a total volume of an Eulerian cell

α_f = Volume fractions of the fuel particle with respect to the total volume in an Eulerian cell

ρ_g' = Macroscopic densities for the vapor

ρ_l' = Macroscopic densities for the liquid

5.3 Conservation Equations

5.3.1 Mass Equations

Vapor:

$$\frac{\partial \rho_g'}{\partial t} + \nabla \cdot \left(\rho_g' u_g \right) = \Gamma_e - \Gamma_c \tag{5.8}$$

Liquid:

$$\frac{\partial \rho_l'}{\partial t} + \nabla \cdot \left(\rho_l' u_l \right) = -\left(\Gamma_e - \Gamma_c \right) \tag{5.9}$$

where u_g = Velocity of vapor field

u_l = Velocity of liquid field

Γ_e = Evaporation rate

Γ_c = Condensation rate

5.3.2 Momentum Equations

Vapor:

$$\rho_g' \frac{\partial u_g}{\partial t} + \rho_g' u_g \frac{\partial u_g}{\partial x} = -\rho_g' g - \alpha_g \frac{\partial P}{\partial x} + K_{gl}\left(u_l - u_g \right) - K_{wg} u_g - V_g + A_m \frac{\partial}{\partial t}\left(u_l - u_g \right) - \Gamma_e \left(u_g - u_l \right) + M_{gp} \tag{5.10}$$

Liquid:

$$\rho_l' \frac{\partial u_l}{\partial t} + \rho_l' u_l \frac{\partial u_l}{\partial x} = -\rho_l' g - \alpha_l \frac{\partial P}{\partial x} + K_{gl}\left(u_g - u_l \right) - K_{wl} u_l - V_l + A_m \frac{\partial}{\partial t}\left(u_g - u_l \right) - \Gamma_e \left(u_l - u_g \right) + M_{lp} \tag{5.11}$$

Fuel Particle:

$$M_{pk}\frac{du_{pk}}{dt} = -M_{pk}g + D_k\left(u_g - u_{pk}\right) + E_k\left(u_l - u_{pk}\right) \tag{5.12}$$

where g = Gravity

P = Pressure

K_{gl} = Vapor-liquid macroscopic drag coefficient

K_{wg} = Wall-vapor friction coefficient

K_{wl} = Wall-liquid friction coefficient

V_g = Viscous loss term for vapor field

V_l = Viscous loss term for liquid field

A_m = Transient virtual mass force coefficient

M_{pk} = Fuel particle mass

M_{gp} = Summation of vapor-Lagrangian particle drags

M_{lp} = Summation of liquid-Lagrangian particle drags

D_k = Vapor-Lagrangian particle drag term

E_k = Liquid- Lagrangian particle drag term

5.3.3 Energy Equations

Vapor:

$$\frac{\partial(\rho_g' I_g)}{\partial t} + \frac{\partial(\rho_g' I_g u_g)}{\partial x} = -P\left[\frac{\partial \alpha_g}{\partial t} + \frac{\partial}{\partial x}\left(\alpha_g u_g\right)\right] + W_g + Q_{gw} + Q_{gp} + Q_{gi}$$

$$-C_g + S_g + \left(\Gamma_e - \Gamma_c\right)h_{gs} \tag{5.13}$$

Liquid:

$$\frac{\partial(\rho_l' I_l)}{\partial t} + \frac{\partial(\rho_l' I_l u_l)}{\partial x} = -P\left[\frac{\partial \alpha_l}{\partial t} + \frac{\partial}{\partial x}\left(\alpha_l u_l\right)\right] + W_l + Q_{lw} + Q_{lp} + Q_{li}$$

$$-C_l + S_l + \left(\Gamma_c - \Gamma_e\right)h_{ls} \tag{5.14}$$

Fuel Particles:

$$M_{pk}\frac{dI_{pk}}{dt} = R_{lk}\left(T_l - T_{pk}\right) + R_{gk}\left(T_g - T_{pk}\right) + R_{ik}\left(T_{sat} - T_{pk}\right) + R_{wk}\left(T_w - T_{pk}\right) + S_{pk} \tag{5.15}$$

where I_g = Internal energy of vapor field

I_l = Internal energy of liquid field

I_{pk} = Internal energy of Lagrangian particle

W_g = Viscous work for vapor

W_l = Viscous work for liquid

Q_{gw} = Wall-vapor heat transfer term

Q_{lw} = Wall-liquid heat transfer term

Q_{gp} = Vapor- Lagrangian particle heat transfer term

Q_{lp} = Liquid- Lagrangian particle heat transfer term

Q_{gi} = Vapor- interface heat transfer term

Q_{li} = Liquid- interface heat transfer term

C_g = Conduction heat transfer term for vapor

C_l = Conduction heat transfer term for liquid

h_{gs} = Vapor enthalpy at saturation temperature

h_{ls} = Liquid enthalpy at saturation temperature

S_g = Heat source term for vapor

S_l = Heat source term for liquid

S_{pk} = Heat source term for Lagrangian particle

T_g = Vapor temperature

T_l = Liquid temperature

T_{pk} = Lagrangian particle temperature

T_w = Wall temperature

T_{sat} = Saturation temperature

R_{gk} = Macroscopic heat transfer coefficient between vapor and Lagrangian particles of kth group

R_{lk} = Macroscopic heat transfer coefficient between liquid and Lagrangian particles of kth group

R_{ik} = Macroscopic heat transfer coefficient between vapor-liquid interface and Lagrangian particles of kth group

R_{wk} = Macroscopic heat transfer coefficient between wall and Lagrangian particles of kth group

5.4 Fragmentation Model

The key constitutive relation in TEXAS is the hydrodynamic fuel fragmentation. Chu [41] developed this model based on a multi-step fragmentation theory for the liquid particles. The model considers the fuel particles to be deformed and dynamically fragmented into the discrete number of particles from its initial diameter to smaller sizes. The complete process of the fragmentation of the fuel in an interaction with the coolant is the result from three mechanisms, (1) Rayleigh-Taylor instability, (2) Kelvin-Helmholtz instability, and (3) boundary layer stripping.

5.4.1 Fragmentation by Rayleigh-Taylor instability

A correlation of this theoretical model for fragmentation is:

$$D(T^+) = D(0)\exp(-C_1(T^+)^{C_2} We^{C_2} \qquad (5.16)$$

where $D(T^+)$ = Fuel diameter at time T^+

$D(0)$ = Fuel diameter at time zero

We = Weber number of the fuel particles

C_1, C_2 = Constants.

The correlation is simplified to a linear time-independent form:

$$D_f^{n+1} = D_f^n(1 - C_0 \Delta T^+ We^{0.25}) \tag{5.17}$$

where n = Old time stamp

$n+1$ = New time step

ΔT^+ = Dimensionless time step

C_0 = Constants.

And

$$We = \frac{\rho_c U_{rel}^2 D_f^n}{\sigma_f} \tag{5.18}$$

$$\Delta T^+ = \frac{U_{rel}(t^{n+1} - t^n)}{D_f^n}\left(\frac{\rho_c}{\rho_f}\right)^{1/2} \tag{5.19}$$

$$C_0 = 0.1093 - 0.0785\left(\frac{\rho_c}{\rho_f}\right)^{1/2} \tag{5.20}$$

5.4.2 Fragmentation by Kelvin-Helmholtz instability

There are two sets of equations to be applied based on the condition of the coolant surrounding the fuel [42]. If the coolant is mostly liquid (void fraction < 0.2, by default), the condition is considered that of a "thin film." That is there is only a very thin vapor film over the surface of the fuel. In such case, the major effect is due to the liquid itself. On the other hand, if the coolant is a mixture of vapor and liquid (void fraction > 0.2) then the "thick film" condition is assumed. In this condition, both liquid and the vapor can affect the fragmentation. Two equations are as followed:

Thin film

$$n_{\max}^2 = \frac{\rho_f \rho_l k_{\min}^2 (u_l - u_f)^2}{(\rho_f + \rho_l)^2} - \frac{(\sigma_f - \sigma_l) k_{\min}^3}{\rho_f + \rho_l} \tag{5.21}$$

and

$$k_{\min} = \frac{2\rho_f \rho_l (u_l - u_f)^2}{3(\rho_f + \rho_l)(\sigma_f + \sigma_l)} \tag{5.22}$$

Thick film

$$n_{\max}^2 = \frac{\rho_f \rho_g k_{\min}^2 (u_g - u_f)^2}{(\rho_f + \rho_g)^2} - \frac{\sigma_f k_{\min}^3}{\rho_f + \rho_g} \quad (5.23)$$

and $$k_{\min} = \frac{2\rho_f \rho_g (u_g - u_f)^2}{3(\rho_f + \rho_g)\sigma_f} \quad (5.24)$$

with $$\lambda_{\max} = \frac{2\pi}{k_{\min}} \quad (5.25)$$

then $$\dot{m}_{KH} = C_0 A \rho_f n_{\max} \lambda_{\max} \quad (5.26)$$

where $\dot{m}_{KH}$ = Fragmentation rate (kg/s) by Kelvin-Helmholtz instability

$n_{\max}$ = Instability's growth rate (/s)

$k_{\min}$ = Instability's smallest wave number (/m)

$\lambda_{\max}$ = Instability's largest wave length (m)

σ = Surface tension (N/m)

ρ_f = Density of the fuel (kg/m^3)

C_0 = Effectiveness of the Kelvin-Helmholtz instability on breaking up the molten fuel. This constant determined by experiments.

A = Surface area of the jet

The sizes of the particles generated from this fragmentation are assumed to be given by the critical Weber number:

$$D_{critical} = \frac{\sigma_f We_{critical}}{\rho_c u_{rel}^2} \quad (5.27)$$

where $We_{critical}$ = The Weber number in which the particles become stable.

$D_{critical}$ = The diameter according to the given critical Weber number (m)

ρ_c = Average density of the coolant (kg/m^3)

5.4.3 Fragmentation by the Boundary Layer Stripping

TEXAS model assumed that the layer of the melt formed at the frontal part of the jet would flow from the frontal part of the jet to the rear and then is stripped away by the surrounding fluid. Chu [41] estimated the erosion rate as:

$$\dot{m}_{BL} = \rho_f \int_{R-\delta}^{R} 2\pi urdr \tag{5.28}$$

with

$$\delta = \left(\frac{2\pi R v_f}{u_{rel}} \right)^{1/2} \tag{5.29}$$

and

$$u = u_{rel} \cdot e^{\frac{(r-R)}{\delta}} \tag{5.30}$$

where $\dot{m}_{BL}$ = Fragmentation rate in kg/s by boundary layer stripping

δ = Boundary layer thickness (m)

u = Velocity (m/s)

u_{rel} = Relative velocity of the fuel and the coolant (m/s)

R = Radius of the jet (m)

The size of the particles generated from the thickness δ eroded is assumed to be that given by Eq.5.27.

5.5 Phase Change Model

The phase change model is an important constitutive relation in TEXAS, which calculates the evaporation rate and the condensation rate, used in the conservation equations. The model assumes that the phase change occurs at the interface of the coolant liquid and vapor, and considers all forms of heat transfer between the fuel and coolant under different flow regime conditions. Generally, the fuel heat is used in three ways:

1. to increase the internal energy of the coolant liquid
2. to increase the internal energy of the coolant vapor
3. to vaporize the coolant liquid.

The energy balance of the fuel can be written:

$$\dot{q}_{net,f} = \dot{q}_f - \dot{q}_l - \dot{q}_g \tag{5.31}$$

where $\dot{q}_f$ = The heat lost by the fuel

$\dot{q}_l$ = The heat received by the coolant liquid

$\dot{q}_g$ = The heat received by the coolant vapor

The detailed description of these heat transfer terms is given in Chu [41]. With the known net heat flow, the phase change rate per unit volume can be calculated:

$$\dot{m}_g = \frac{\dot{q}_{net,f}}{h_{fg} V_{cell}} \tag{5.32}$$

where h_{fg} = Latent heat for the coolant

V_{cell} = Volume of an Eulerian cell

If the net heat flow is positive, coolant liquid is vaporized. And the evaporation rate is:

$$\Gamma_e = \dot{m}_g \quad \text{and} \quad \Gamma_c = 0 \tag{5.33}$$

But if the net heat flow is negative, coolant vapor is condensed. And the condensation rate is:

$$\Gamma_e = 0 \quad \text{and} \quad \Gamma_c = \dot{m}_g \tag{5.34}$$

5.6 Fuel Surface Temperature

Each fuel particle is assumed to have two uniform temperatures: (1) temperature at the center and (2) temperature at the surface with the thickness determined by a thermal layer. The thermal layer thickness, δ, is calculated based on average thickness of heat conduction for a plate, which is:

$$\delta = \frac{2}{3}\sqrt{\pi\alpha\beta_{mix}} \tag{5.35}$$

where α = Thermal diffusivity

β_{mix} = Time for mixing

The heat transfer through the thermal layer is by conduction:

$$AK\frac{T_p^{n+1} - T_s^{n+1}}{\delta} = \dot{Q}_{out} \tag{5.36}$$

where A = Particle surface area

K = Conductivity of the fuel particle

T_p^{n+1} = Center temperature of the fuel particle at time new time step

T_s^{n+1} = Surface temperature of the fuel particle at time new time step

$\dot{Q}_{out}$ = Total heat flow rate from the fuel to the coolant

But the fuel particle energy loss is:

$$M_p\frac{I_p^{n+1} - I_p^n}{\Delta t} = -\dot{Q}_{out} \tag{5.37}$$

where M_p = Mass of the fuel particle

I_p^{n+1} = Internal energy of the fuel particle at new time step

I_p^n = Internal energy of the fuel particle at current time step

Δt = Run time step

The internal energy is a function of the particle temperature:

$$I_p^{n+1} = I_{ref} + C_p(T_p^{n+1} - T_{ref}) \tag{5.38}$$

Solving Eq. 5.36-5.38, the surface temperature can be expressed:

$$T_s^{n+1} = T_p^n - \dot{Q}_{out}\left\{\frac{\Delta t}{M_p C_p} + \frac{\delta}{AK}\right\} \tag{5.39}$$

5.7 Approximation of the latent heat

$$h_{fg} = h_{gs} - h_f \tag{5.40}$$

where h_{gs} = Enthalpy of the saturated vapor

h_f = Enthalpy of the saturated liquid

And

$$h_{gs} = i_{gs} + Pv_{gs} \tag{5.41}$$

$$h_f = i_f + Pv_f \tag{5.42}$$

where i_{gs} = Internal energy of the saturated vapor

P = Local pressure of the Eulerian cell

v_{gs} = Specific volume of the saturated vapor

i_f = Internal energy of the liquid

v_f = Specific volume of the liquid

Because $i_f >> Pv_f$, then

$$h_f \approx i_f \tag{5.43}$$

Substituting h_{gs} and h_f into Eq. 5.40, then

$$h_{fg} = i_{gs} + Pv_{gs} - i_f \tag{5.44}$$

5.8 Further Modification

Before applying the TEXAS model used in the high temperature process into the water-liquid nitrogen interaction, the modification on the code is needed. The modified parts of TEXAS are given in Appendix B. This modification is briefly described below:

1. The state properties
   - 1.1 Gas_internalenergysat function
   - 1.2 Gas_internalenergy function
   - 1.3 Gas_internalenergyreset function
   - 1.4 Gas_tempsat function
   - 1.5 Gas_temp function
   - 1.6 Gas_density function
   - 1.7 Gas_specheat function
   - 1.8 Gas_recipsoundspeedsq function
   - 1.9 Setupmix subroutine
   - 1.10 Hsatf function
   - 1.11 Setc subroutine

Eleven functions above are related to the thermodynamic properties of the coolant. The original TEXAS code use the water for coolant in the high temperature experiment while, in this dissertation the liquid nitrogen is used. Thus, the modification is required to handle the usage of the liquid nitrogen as the coolant.

2. Qwall subroutine

This original subroutine is modified to correct the error due to the mismatching in unit of some variables related to the heat transfer coefficient from the wall to the vapor or the liquid. Basically, at high temperature the heat transfer between the vessel wall and the interaction inside the vessel by this subroutine can be neglected, so that

this error is automatically insignificant. However, as the wall heating is more effective for the process at the low temperature, this error must be corrected.

3. Evpcod subroutine

This subroutine calculates the evaporation rate and the condensation rate. The subroutine neglects the evaporation and condensation effect in the Eulerian cells that the fuel disappears. This assumption greatly reduces the run time required for the entire interaction by giving an approximated result. However, the assumption overrules the conservation equations. The modification treats the evaporation and condensation of all cells into account to agree with the conservation equations.

4. Heatlg subroutine

This subroutine calculates the heat transfer coefficient between the vapor to the vapor/liquid interface and the heat transfer coefficient between the interface to the liquid. Each Eulerian cells is initially assigned the heat transfer between these interface even though a droplet does not exist in a vapor cell (void fraction = 1) or a bubble does not exist in the liquid cell (void fraction = 0). The modification is to correct this error by checking the minimum void fraction or the maximum void fraction before calculating the heat transfer coefficient between these interfaces.

5. Main program

This modification is to re-order the flow of the code such that the Qwall subroutine is implemented before calculating the evaporation and the condensation rate in the following subroutine, Evpcod.

6. Newfrag subroutine
7. Dks subroutine
8. Echk subroutine

The Newfrag subroutine calculates the fuel fragmentation during the fuel-coolant mixing. The Dks subroutine determines the drag coefficients and the Echk subroutine checks the total energy in the system. Each of these three subroutines has a trivial error that is fixed by the modification. The modification is to fix the error.

5.9 Assumption Notes

Some assumptions are inherently implemented by TEXAS itself and some assumptions are particularly used in this dissertation. They are specified below:

1. Constant specific heat of water.
2. Constant specific heat of ice.
3. Constant and equal density for water and ice.
4. Constant viscosity of water, liquid nitrogen and gaseous nitrogen.
5. Constant surface tension coefficient of water and liquid nitrogen.
6. Melting temperature 273.16 and internal energy is zero.
7. Solidifying temperature 273.15 and internal energy is –333 kJ/kg.
8. Initial zero velocity of the liquid and vapor in all Eulerian cells; hence the zero Reynolds number, the dominated laminar heat transfer coefficient, and the zero turbulent convection heat transfer coefficient; also the zero viscous work.
9. No other gas inside the chamber except the nitrogen gas.
10. Fuel particle velocity is set to zero when contacting the bottom of the chamber, and the fuel particle combines with the previous particle if its temperature is greater or equal to its melting temperature.
11. Pressure built up during the water injection does not change the constant injection speed.
12. Volume of the guide tube is small and is neglected.
13. No heat transfer from the bottom end of the chamber.

5.10 Simulation tests

The simulation tests are executed with their test conditions shown in Table 5.1, and the input file for each test is shown in Appendix C. The data of the velocity of the injected water is approximated from the pre-experiment conducted without the liquid nitrogen. In practice, the velocity of the injected water decreases with time due to the decreasing amount of the water in the bottle, the friction along the valves and the guide tube and the back-pressure generated from the interaction inside the chamber.

Table 5.1 Simulation test conditions

Water injection pressure (bar)	Injected Water Velocity (m/s)	Initial water to liquid nitrogen volumetric ratio
2	0.88	0.05
2	0.52	0.10
3	0.89	0.05
3	1.29	0.10
3	1.62	0.15
3	1.84	0.20
4	1.66	0.05
4	2.19	0.10
4	2.42	0.15
4	2.62	0.20

5.11 Simulation Results

Before testing the simulation, the initial and the base cases are tested. Fig. 5.1 is the simulation with the initial configuration. The chamber is separated into 25 Eulerian cells starting at Cell 2 to Cell 26. Each cell is 4-cm height. The liquid nitrogen is filled from Cell 2 to Cell 7, which is equal to the intended quantity of the liquid nitrogen in the experiment. Gauge G1-G8 are the instrumental gauges, which can be selected by user to measure the void fraction, pressure, liquid temperature, or vapor temperature at its Eulerian location. The measured values are plotted on the right side of the chamber.

Cell 9 and Cell 26 are correspondent to the position of the pressure transducer (PT1) and the pressure transducer (PT2), respectively. The water injection starts at Cell 9 and flows down to the lower cells.

The void fraction, pressure, liquid temperature, or vapor temperature along the side of the chamber can also be plotted in the left side of the chamber.

Fig. 5.2 is the base case where 1cc 77K of water is injected into the 77K liquid nitrogen inside the chamber with its wall temperature at 77K. The simulated profiles of the pressure and the other values show that there is no transient, which is expected since there is zero heat transferred in the system.

Fig. 5.3 and 5.4 show the case where 1cc 77K of water is injected into the 77K liquid nitrogen inside the chamber with an assumed wall temperature of 273K. The simulated profiles of the pressure during the first 0.4 second agree with the experimental pressure profiles during the same period. The 0.4 second is required for water to come down from the solenoid valve to contact with the surface of the liquid nitrogen. The pressurization from the simulation is 0.18 bar per second which ranged from 0.07 to 0.15 bar per second. The deviation of the pressurization from the simulation is 20-160%. The cause of the deviation comes from the initial wall temperature assigned to each Eulerian cell in TEXAS code and the actual environment temperatures which deviate from one to another. Anyway, the scale of the pressurization was very small when compared to the scale of the spike pressurization (6-25 bar per second).

Fig. 5.5-5.14 show the simulations with the test conditions as described in Table 5.1, and the summary data from the simulations and the experiments are shown in Table 5.2. The comparison between $\left(\frac{dp}{dt}\right)_{max}$ in percent and in ratio from the experiments to that from the mixing simulations is summarized in Table 5.3.

5.12 Analyses

The results from the simulation tests show that in the mixing phase the pressure spike does not occurs. In addition, the comparison of the difference in $\left(\frac{dp}{dt}\right)_{max}$ and their ratio are also given in Fig. 5.15 and 5.16.

Both figures show that the $\left(\frac{dp}{dt}\right)_{max}$ from the tests with 2-bar(g) water injection is almost equal to the $\left(\frac{dp}{dt}\right)_{max}$ from the experiments. Therefore, at these 2-bar conditions, the mixing process dominates the interaction.

For the white-dot at 3-bar(g) water injection, the $\left(\frac{dp}{dt}\right)_{max}$ from the experiment is much higher than the $\left(\frac{dp}{dt}\right)_{max}$ from the simulation. The results suggest that the interaction between the water and the liquid nitrogen is dominated by the process that is more energetic than the mixing.

For the black-dot conditions, the $\left(\frac{dp}{dt}\right)_{max}$ from the experiment is much higher than the $\left(\frac{dp}{dt}\right)_{max}$ from the simulation. In percentage, the difference in this case is not much different from that of the white-dot at 3-bar(g) water injection. However, the ratio of $\left(\frac{dp}{dt}\right)_{max}$ clearly distinguishes the black-dot group and the white dot group. The $\left(\frac{dp}{dt}\right)_{max}$ from the experiment is more than twenty five times of that from the simulation and can be as 100 times greater. Such results confirm the possibility of the explosion-liked interaction for the experiment whose condition lies in the black-dot region.

One should takes a little look further to the void fraction profiles in the black-dot case. In Fig. 5.17-5.21, the same simulations had been tried, but the simulations were stopped at the inception times of the pressure spikes as observed from the experiments. The void fraction below 0.9 was observed during the mixing simulation.

In Fig. 5.17 and 5.18, the void fraction from Cell 9 to Cell 26 is nearly 1. This portion of the chamber is filled by the vapor. Thus the sound speed is substantially higher than in the mixture. The results from the simulation explain why the experimental pressure spikes in Fig. 4.2(a) and 4.3(a), which were detected by PT1 and PT2, start increasing nearly at the same time. Note that the water injection for these two cases is still in progress at the inception time since the water is still being injected at Cell 9.

In Fig. 5.19, the water jet is in progress as seen in Cell 9 at the inception time. The void fraction from Cell 5 to Cell 9 lies between 0.1 and 0.5. These results correspond to the experimental analysis. Such void fraction causes the delay time of the pressure spikes as detected by PT1 and PT2 in the experiment. This void fraction was presumed previously in Chapter 4 and is now confirmed by the simulations.

In Fig. 5.20, the void fraction from Cell 4 to Cell 10 lies between 0.1 and 0.5. At this time, the water jet is still in progress as indicated by the injection Cell 9. Due to the longer distance in the mixture, the delay time will be greater than the delay time observed in the previous case. In Fig. 5.22, the pressure profiles from the experiment show that the delay time is 27 ms which is more than twice the delay time of 14 ms in the case of 0.10 volumetric ratio and 4 bar (g) injection. The results from the simulation and the experiment agree to each other.

In Fig. 5.21, the void fraction from Cell 1 to Cell 10 lies between 0.1 and 0.4. But the water injection was already finished. The discrepancy in injection period may come from the initial injection velocity estimated from the injection without the liquid nitrogen as the water-liquid nitrogen interaction increases the pressure inside the chamber and retards the injection velocity. The other possibility is that the injection pressure just after the water injection is strong enough to disturb and trig the interaction inside the chamber.

Table 5.2 Summary data from the simulations and the experiments

Water injection pressure (bar)	Initial water to liquid nitrogen volumetric ratio	Observable spikes from the mixing simulation	Observable spikes from the experiment	$\left(\frac{dp}{dt}\right)_{max}$ during the mixing from the simulation (bar/s)	$\left(\frac{dp}{dt}\right)_{max}$ from experiment (bar/s)
2	0.05	-	-	0.24	0.26
2	0.10	-	-	0.20	0.21
3	0.05	-	✓	0.23	25.0
3	0.10	-	-	0.33	2.89
3	0.15	-	-	0.40	5.70
3	0.20	-	-	0.41	1.26
4	0.05	-	✓	0.25	6.47
4	0.10	-	✓	0.45	23.6
4	0.15	-	✓	0.45	24.8
4	0.20	-	✓	0.55	16.1

Table 5.3 Comparison between $\left(\frac{dp}{dt}\right)_{max}$ in percent and in ratio from the experiments to that of the mixing simulations.

Water injection pressure (bar)	Initial water to liquid nitrogen volumetric ratio	$\left(\frac{dp}{dt}\right)_{max}$ during the mixing from the simulation (bar/s)	$\left(\frac{dp}{dt}\right)_{max}$ from experiment (bar/s)	$\left(\frac{dp}{dt}\right)_{max}$ difference (%)	$\left(\frac{dp}{dt}\right)_{max}$ ratio
2	0.05	0.24	0.26	8	1.1
2	0.10	0.20	0.21	5	1.1
3	0.05	0.23	25.0	99	108.7
3	0.10	0.33	2.89	89	8.8
3	0.15	0.40	5.70	93	14.3
3	0.20	0.41	1.26	67	3.2
4	0.05	0.25	6.47	96	25.9
4	0.10	0.45	23.6	98	52.4
4	0.15	0.45	24.8	98	55.1
4	0.20	0.55	16.1	97	29.3

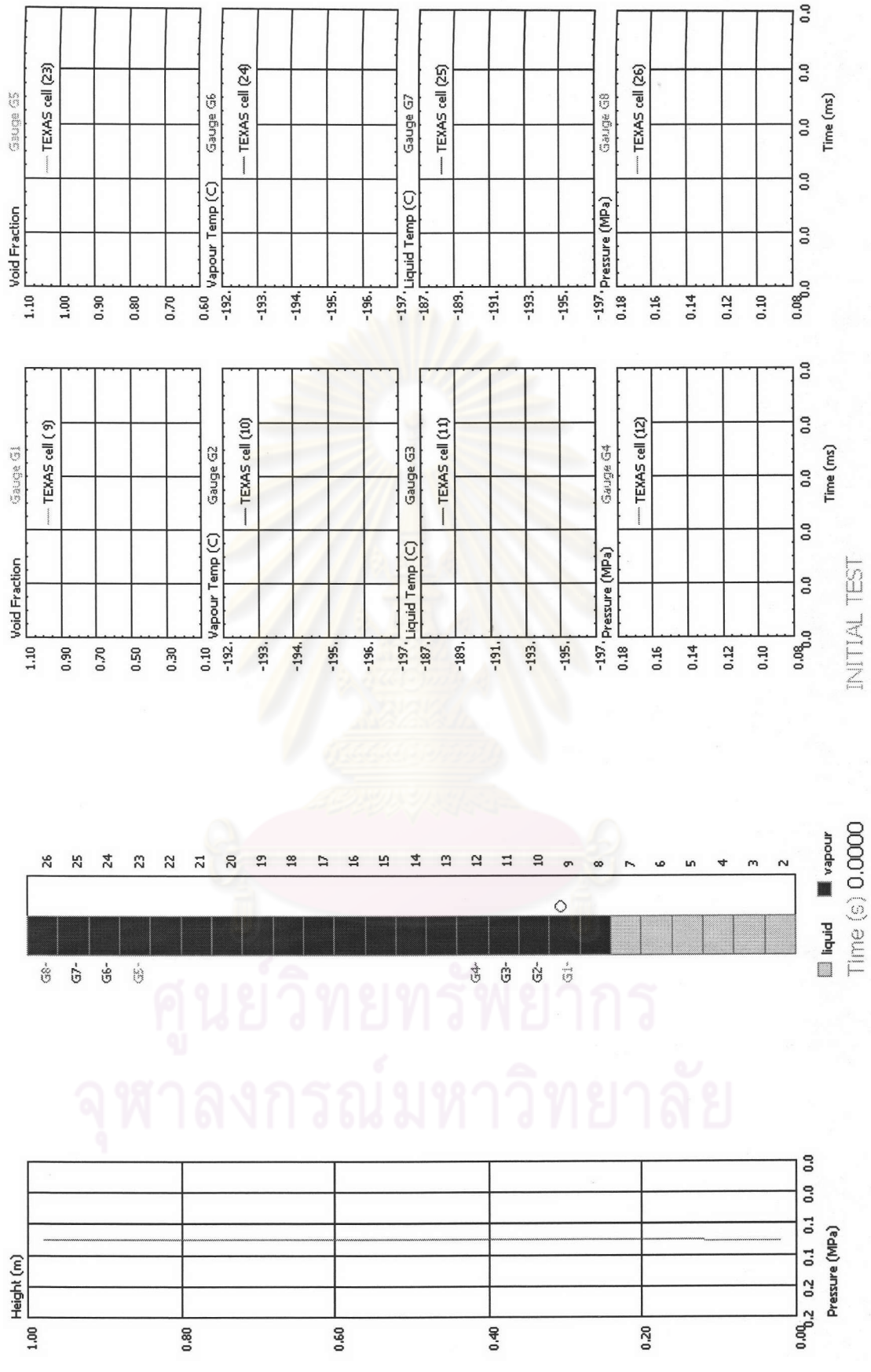

Fig. 5.1 Initial configuration of the experimental model.

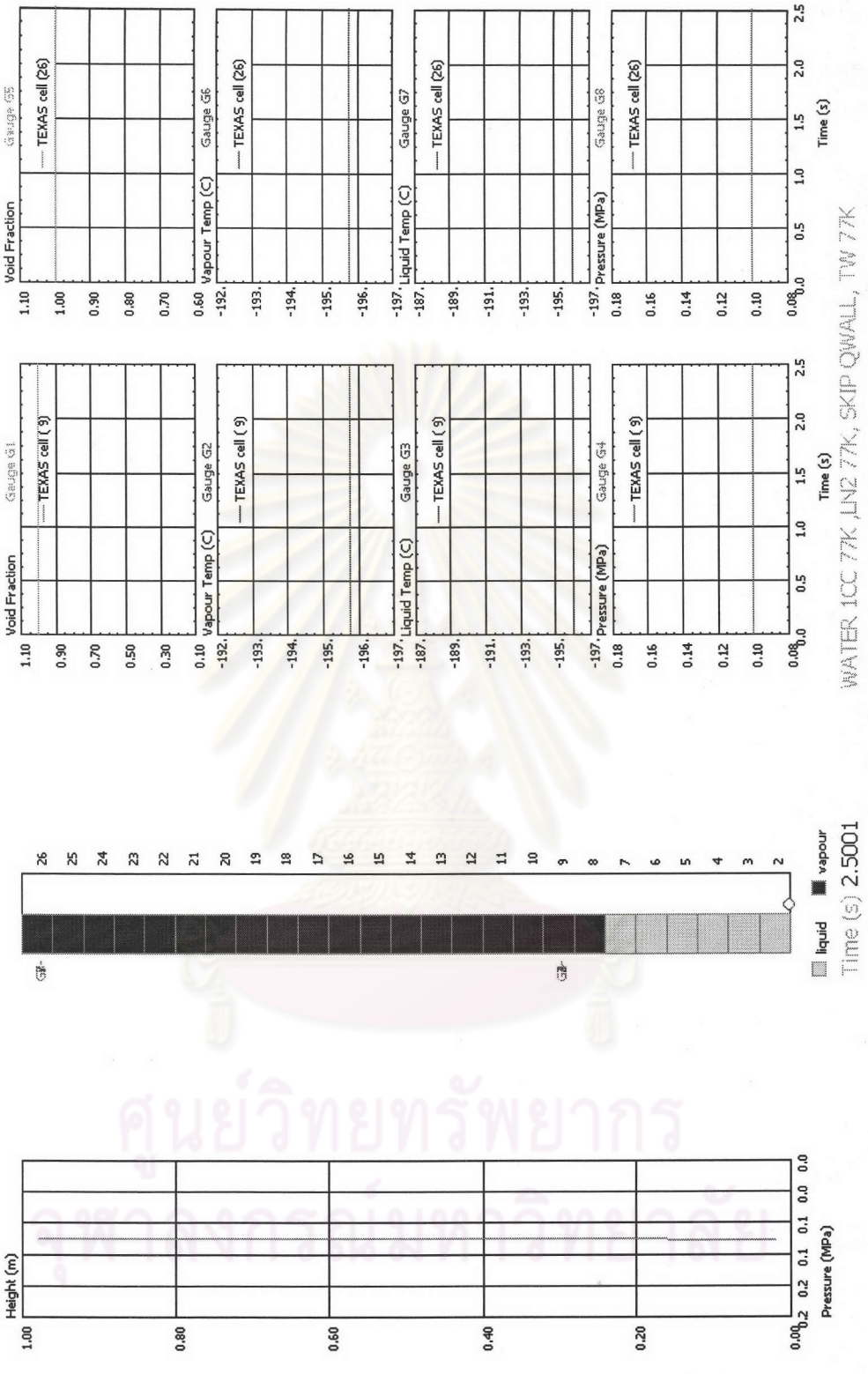

Fig. 5.2 Zero boiling test with test conditions: All initial temperatures of water, nitrogen, and wall in all cells are 77.244 K. The Qwall subroutine is skipped. G1, G2, G3, and G4 measure the properties in Cell 9 while G5, G6, G7, and G8 measure the properties in Cell 26

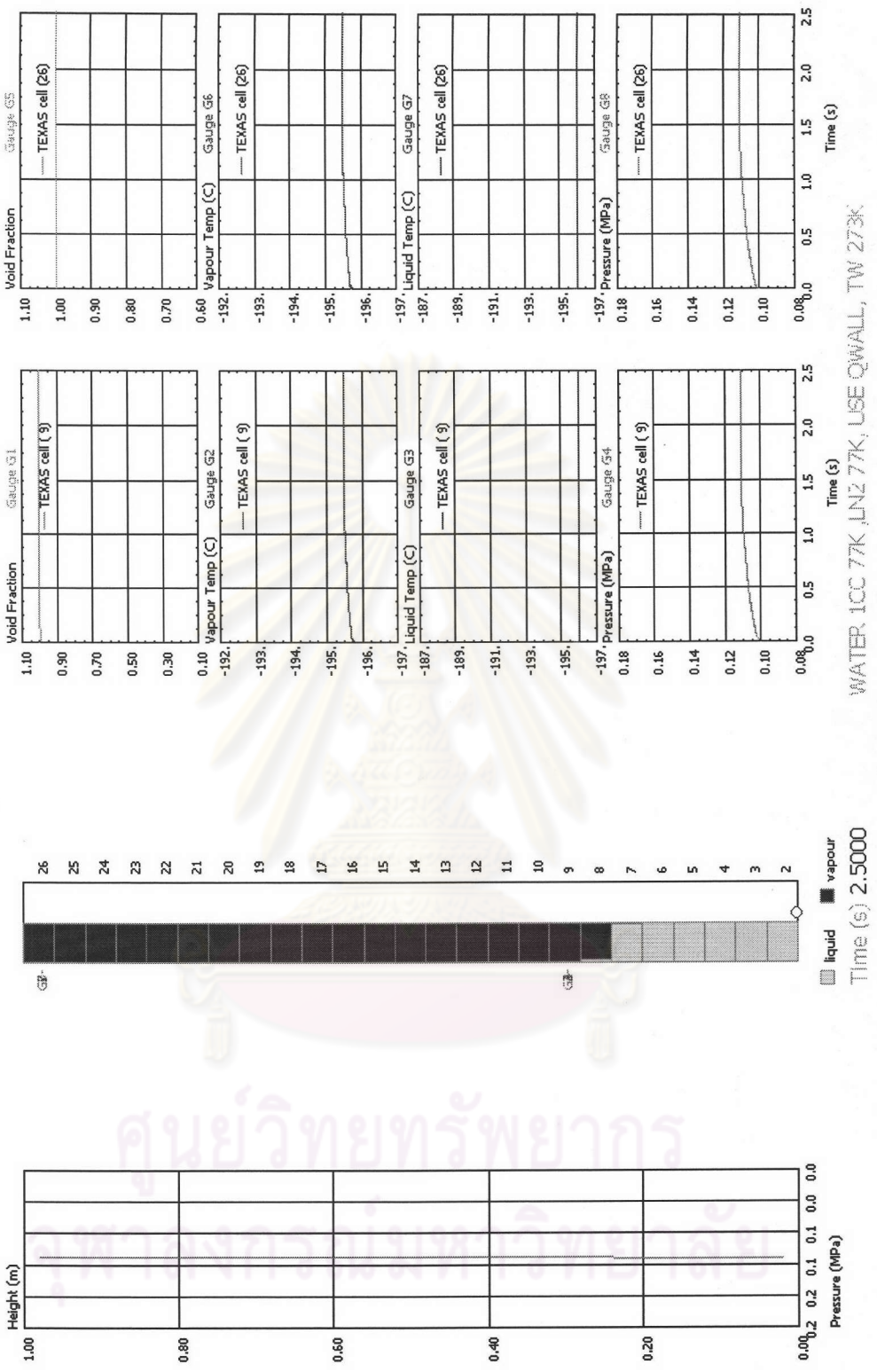

Fig. 5.3 Boiling test with test conditions: Initial water and nitrogen temperatures are 77.244 K. Initial wall temperature is 273 K. The Qwall subroutine is executed. G1, G2, G3, and G4 measure the properties in Cell 9 while G5, G6, G7, and G8 measure the properties in Cell 26

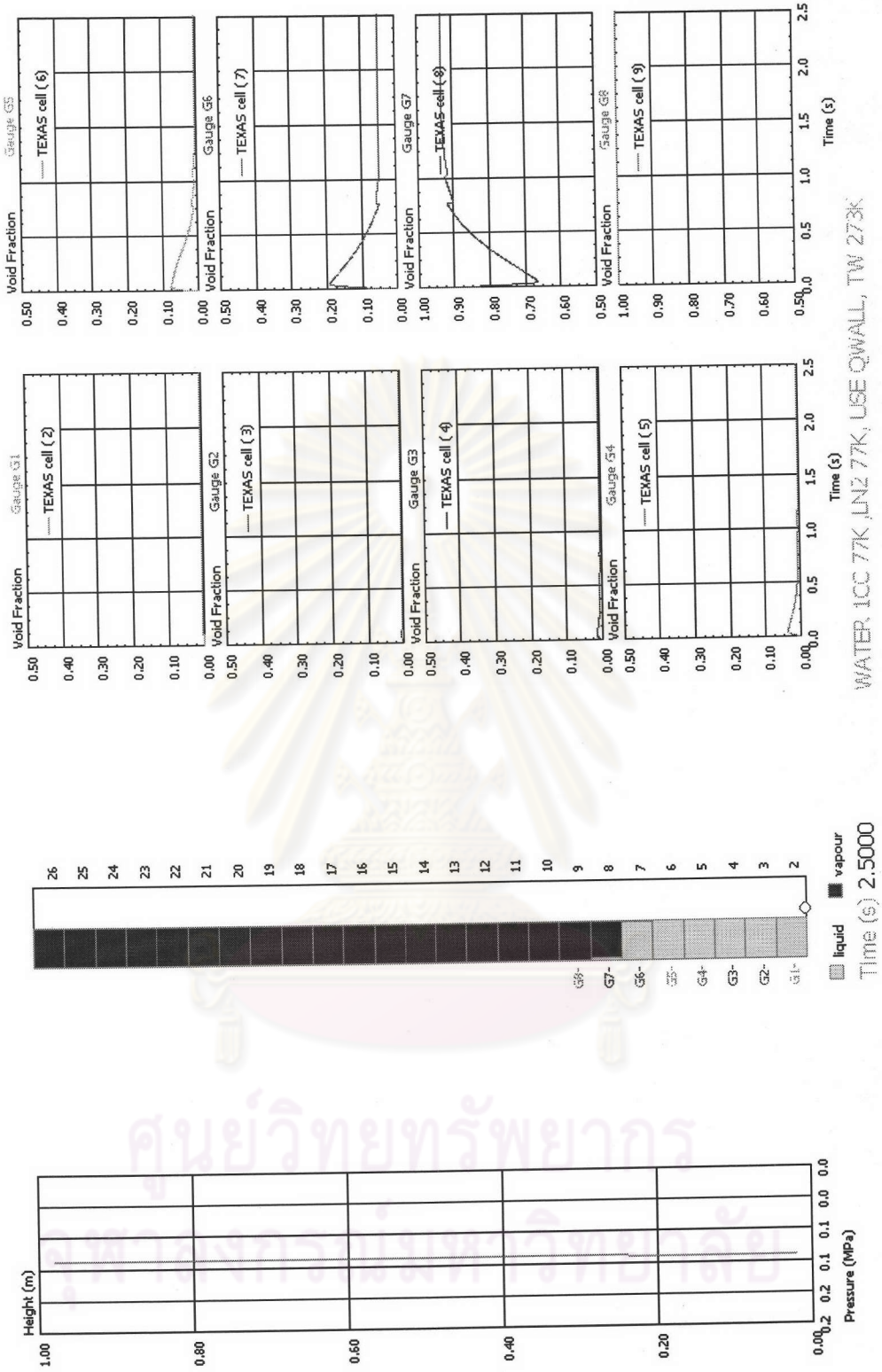

Fig. 5.4 Boiling test with test conditions: Initial water and nitrogen temperatures are 77.244 K. Initial wall temperature is 273 K. The Qwall subroutine is executed. G1 to G8 measure void fraction in cell 2 to Cell 9.

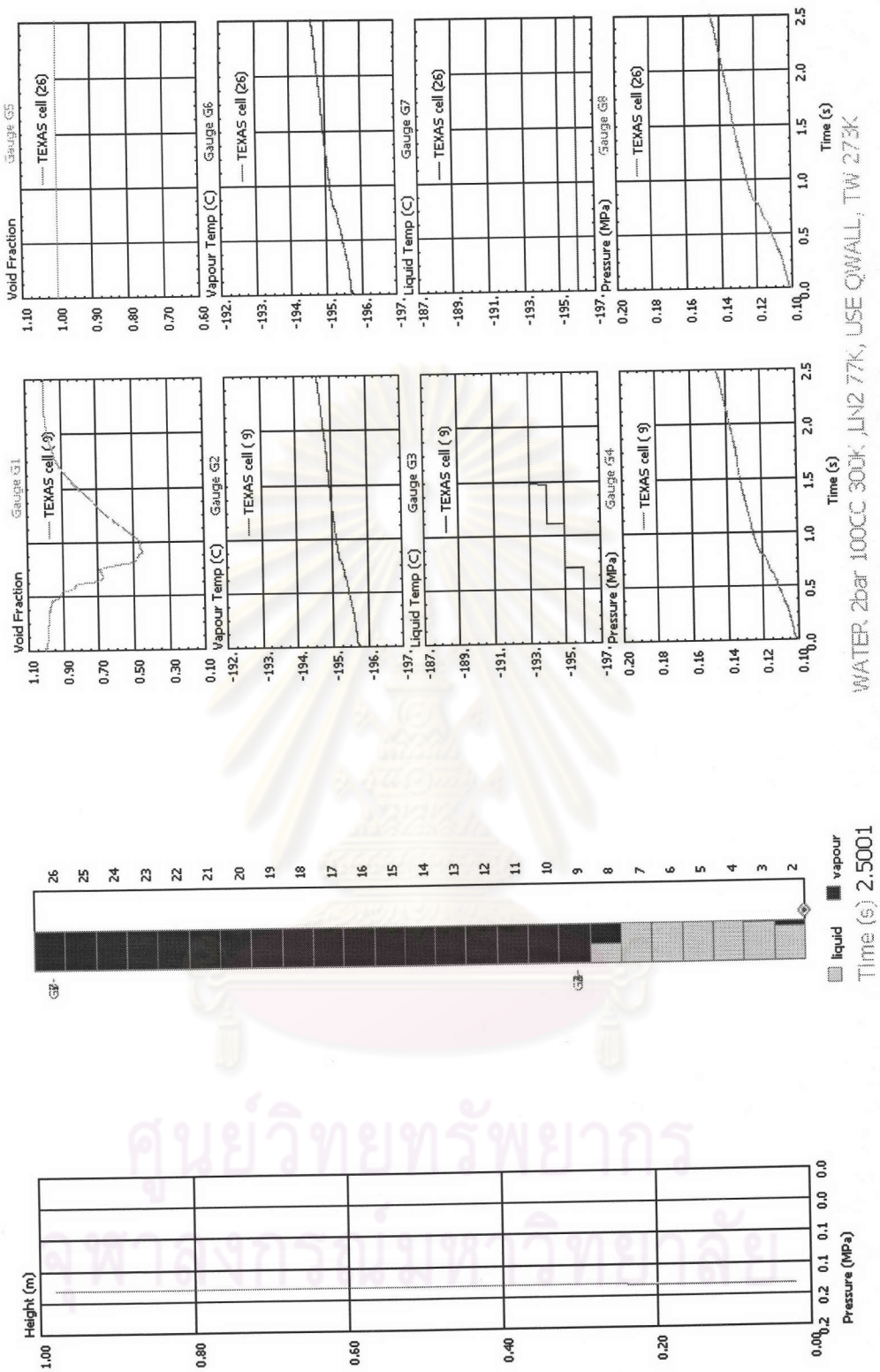

Fig. 5.5 Simulate the experiment with test conditions: Volumetric ratio is 0.05. Water injection pressure is 2 bar. Initial water, nitrogen, and wall temperatures are 300 K, 77.244 K, and 273 K, respectively. G1, G2, G3, and G4 measure the properties in Cell 9 while G5, G6, G7, and G8 measure the properties in cell 26.

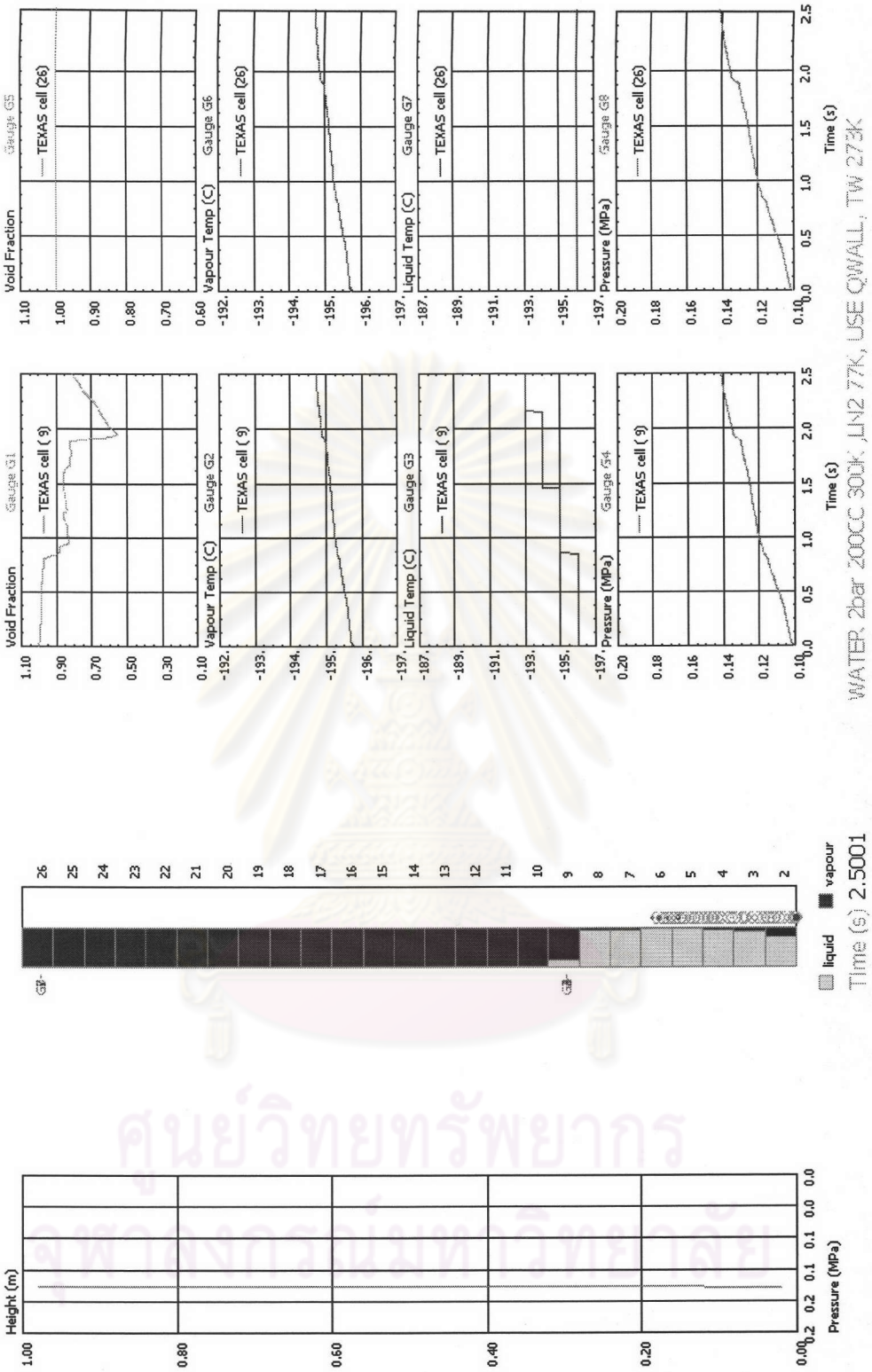

Fig. 5.6 Simulate the experiment with test conditions: Volumetric ratio is 0.10. Water injection pressure is 2 bar. Initial water, nitrogen, and wall temperatures are 300 K, 77.244 K, and 273 K, respectively. G1, G2, G3, and G4 measure the properties in Cell 9 while G5, G6, G7, and G8 measure the properties in cell 26.

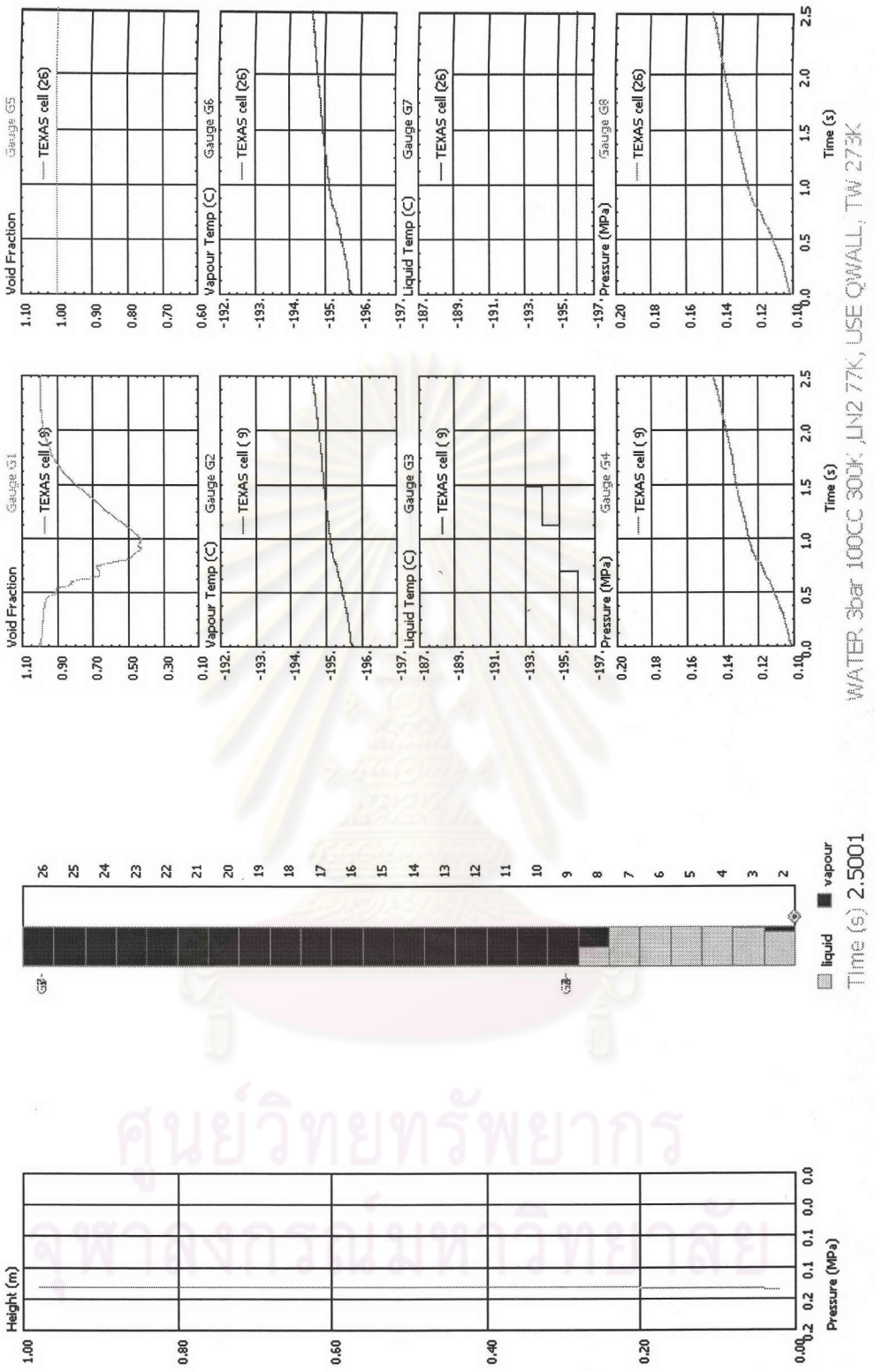

Fig. 5.7 Simulate the experiment with test conditions: Volumetric ratio is 0.05. Water injection pressure is 3 bar. Initial water, nitrogen, and wall temperatures are 300 K, 77.244 K, and 273 K, respectively. G1, G2, G3, and G4 measure the properties in Cell 9 while G5, G6, G7, and G8 measure the properties in cell 26.

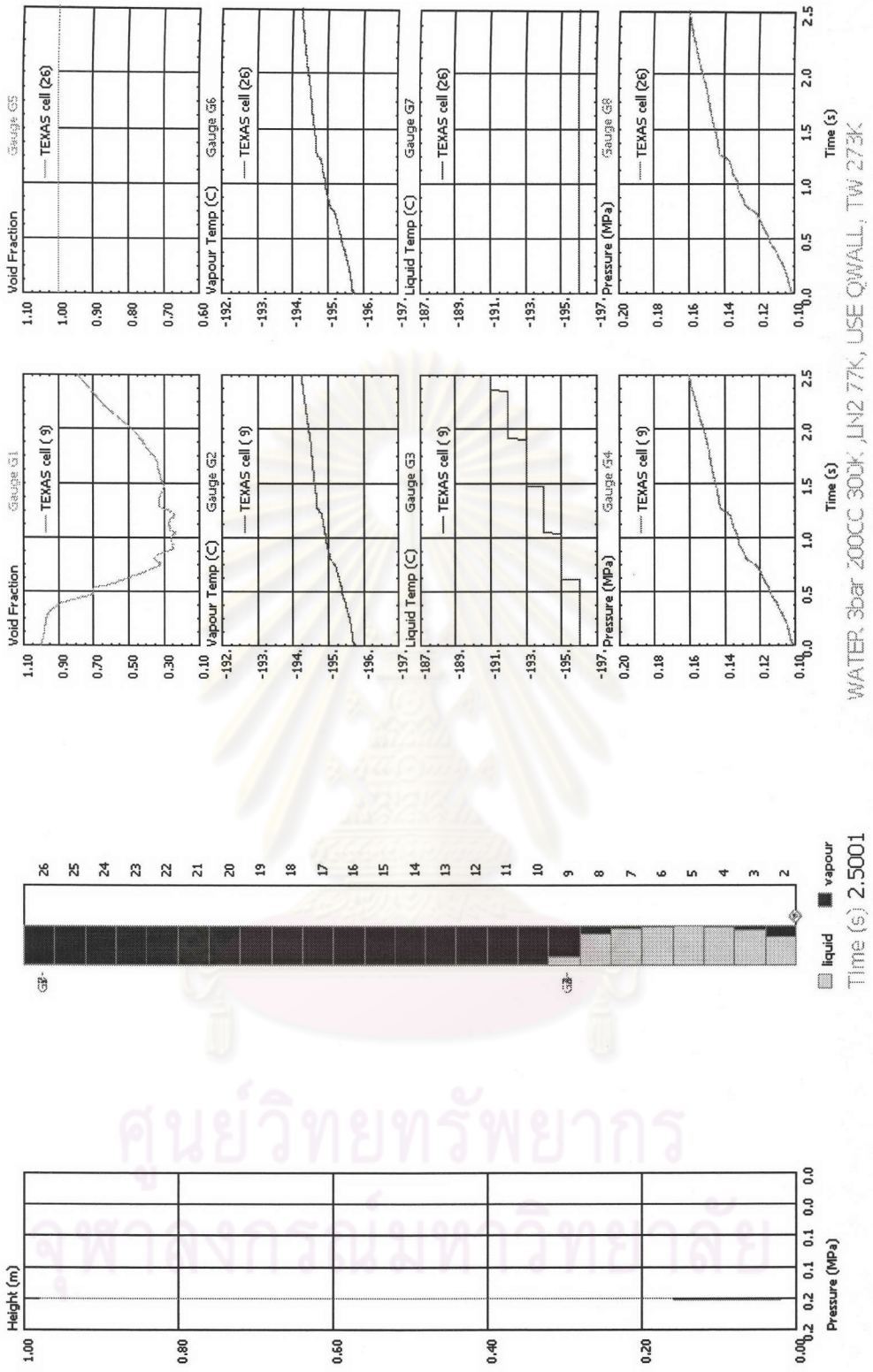

Fig. 5.8 Simulate the experiment with test conditions: Volumetric ratio is 0.10. Water injection pressure is 3 bar. Initial water, nitrogen, and wall temperatures are 300 K, 77.244 K, and 273 K, respectively. G1, G2, G3, and G4 measure the properties in Cell 9 while G5, G6, G7, and G8 measure the properties in cell 26.

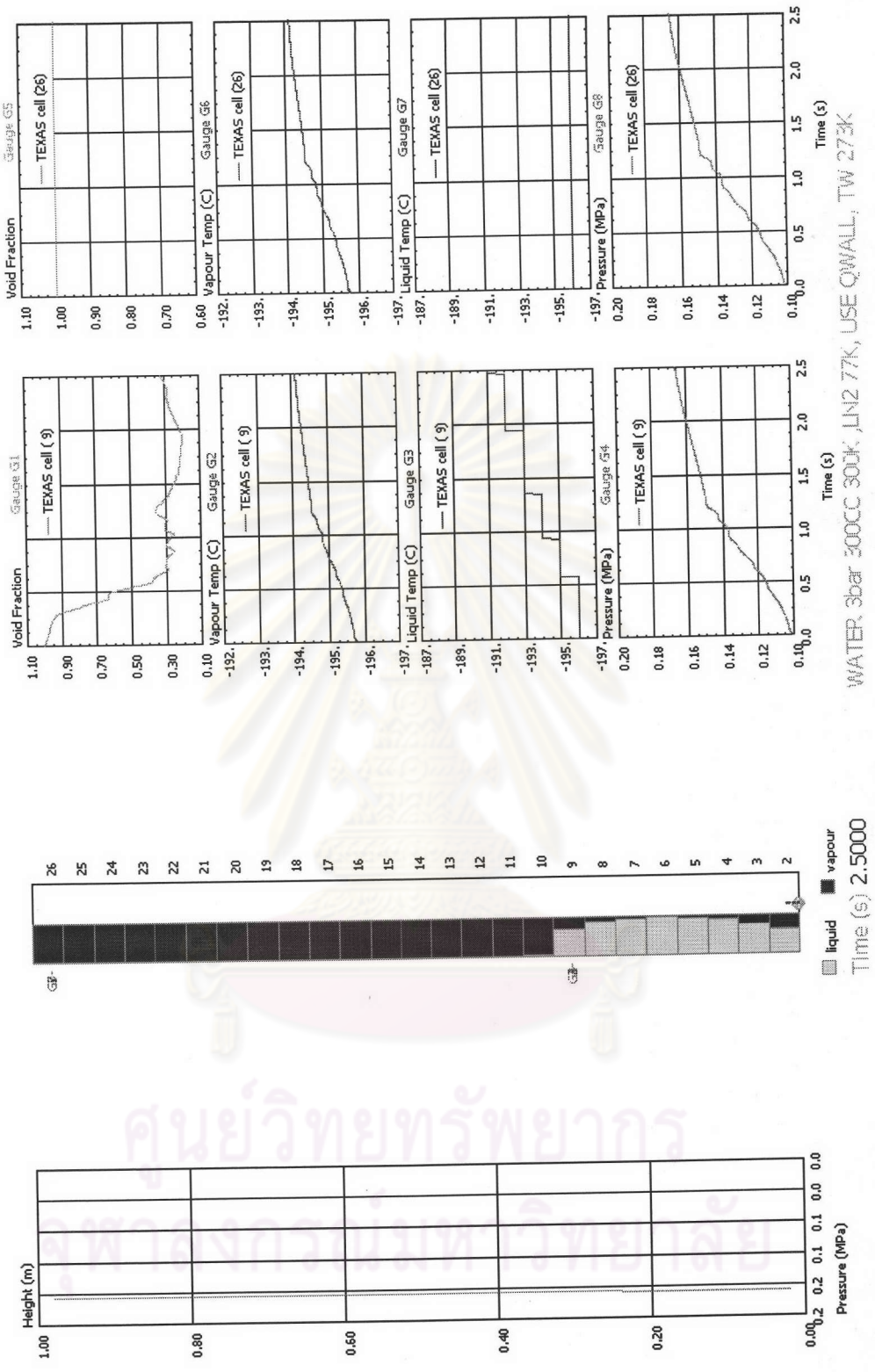

Fig. 5.9 Simulate the experiment with test conditions: Volumetric ratio is 0.15. Water injection pressure is 3 bar. Initial water, nitrogen, and wall temperatures are 300 K, 77.244 K, and 273 K, respectively. G1, G2, G3, and G4 measure the properties in Cell 9 while G5, G6, G7, and G8 measure the properties in cell 26.

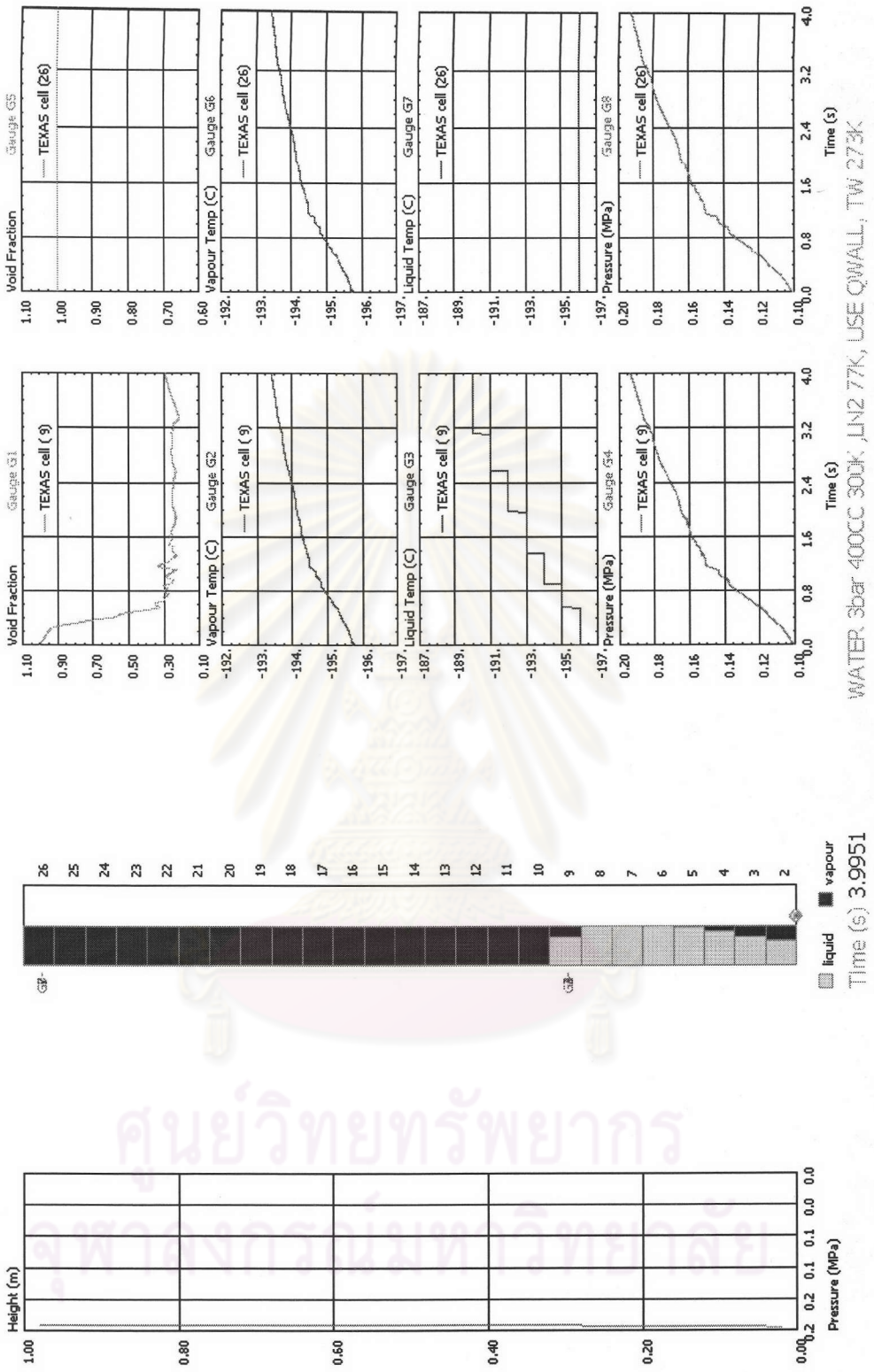

Fig. 5.10 Simulate the experiment with test conditions: Volumetric ratio is 0.20. Water injection pressure is 3 bar. Initial water, nitrogen, and wall temperatures are 300 K, 77.244 K, and 273 K, respectively. G1, G2, G3, and G4 measure the properties in Cell 9 while G5, G6, G7, and G8 measure the properties in Cell 26.

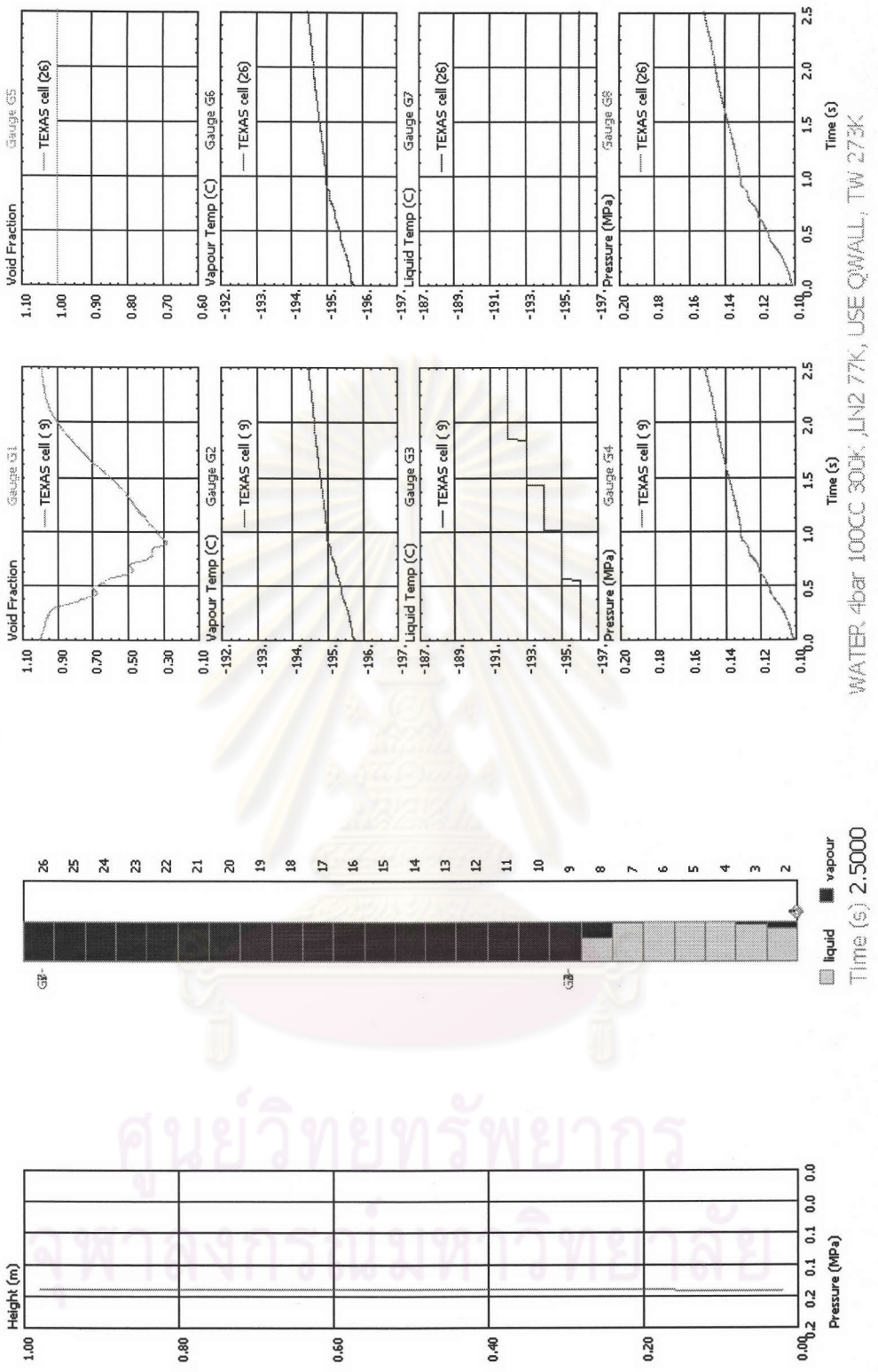

Fig. 5.11 Simulate the experiment with test conditions: Volumetric ratio is 0.05. Water injection pressure is 4 bar. Initial water, nitrogen, and wall temperatures are 300 K, 77.244 K, and 273 K, respectively. G1, G2, G3, and G4 measure the properties in Cell 9 while G5, G6, G7, and G8 measure the properties in Cell 26.

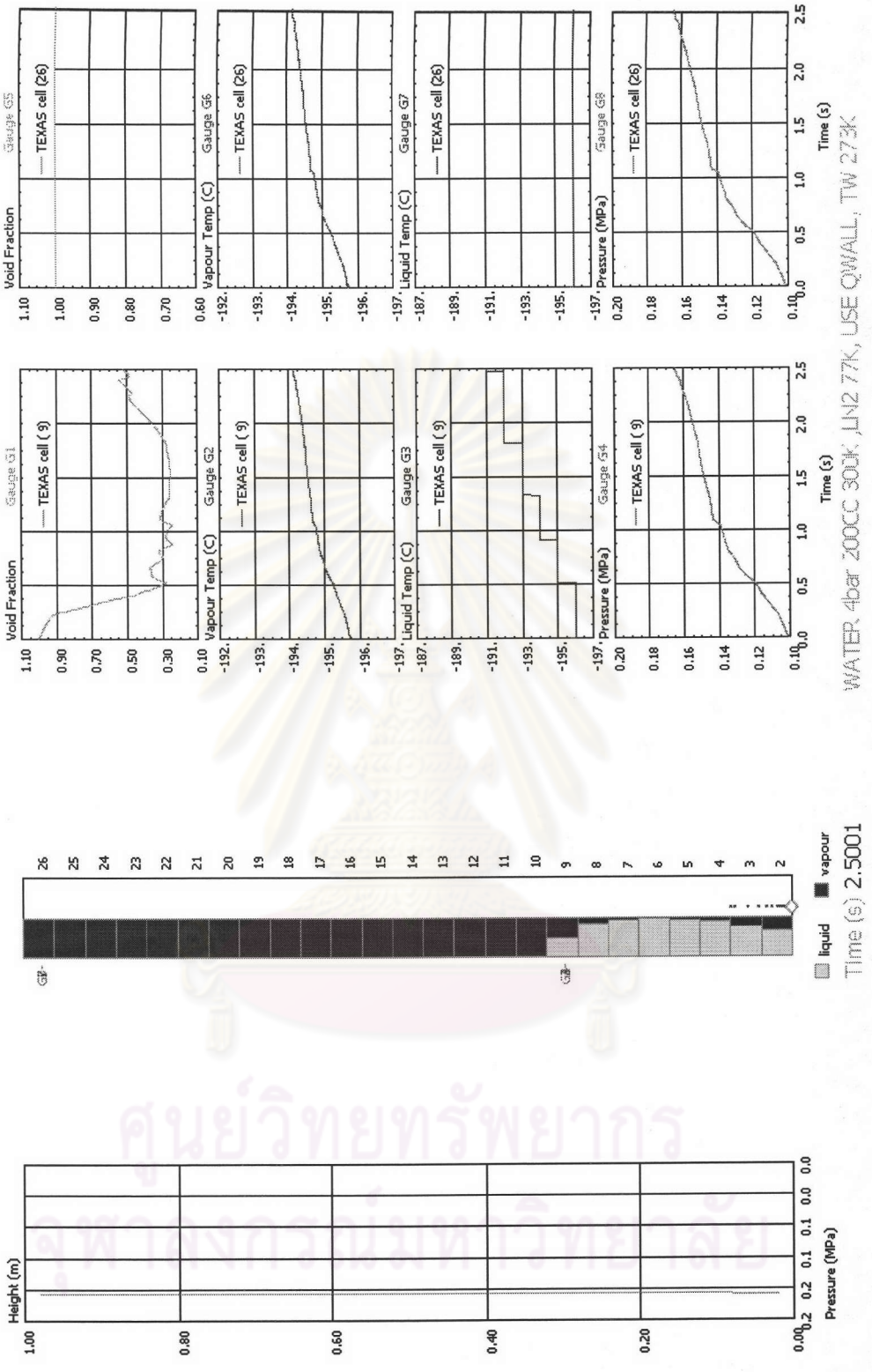

Fig. 5.12 Simulate the experiment with test conditions: Volumetric ratio is 0.10. Water injection pressure is 4 bar. Initial water, nitrogen, and wall temperatures are 300 K, 77.244 K, and 273 K, respectively. G1, G2, G3, and G4 measure the properties in Cell 9 while G5, G6, G7, and G8 measure the properties in Cell 26.

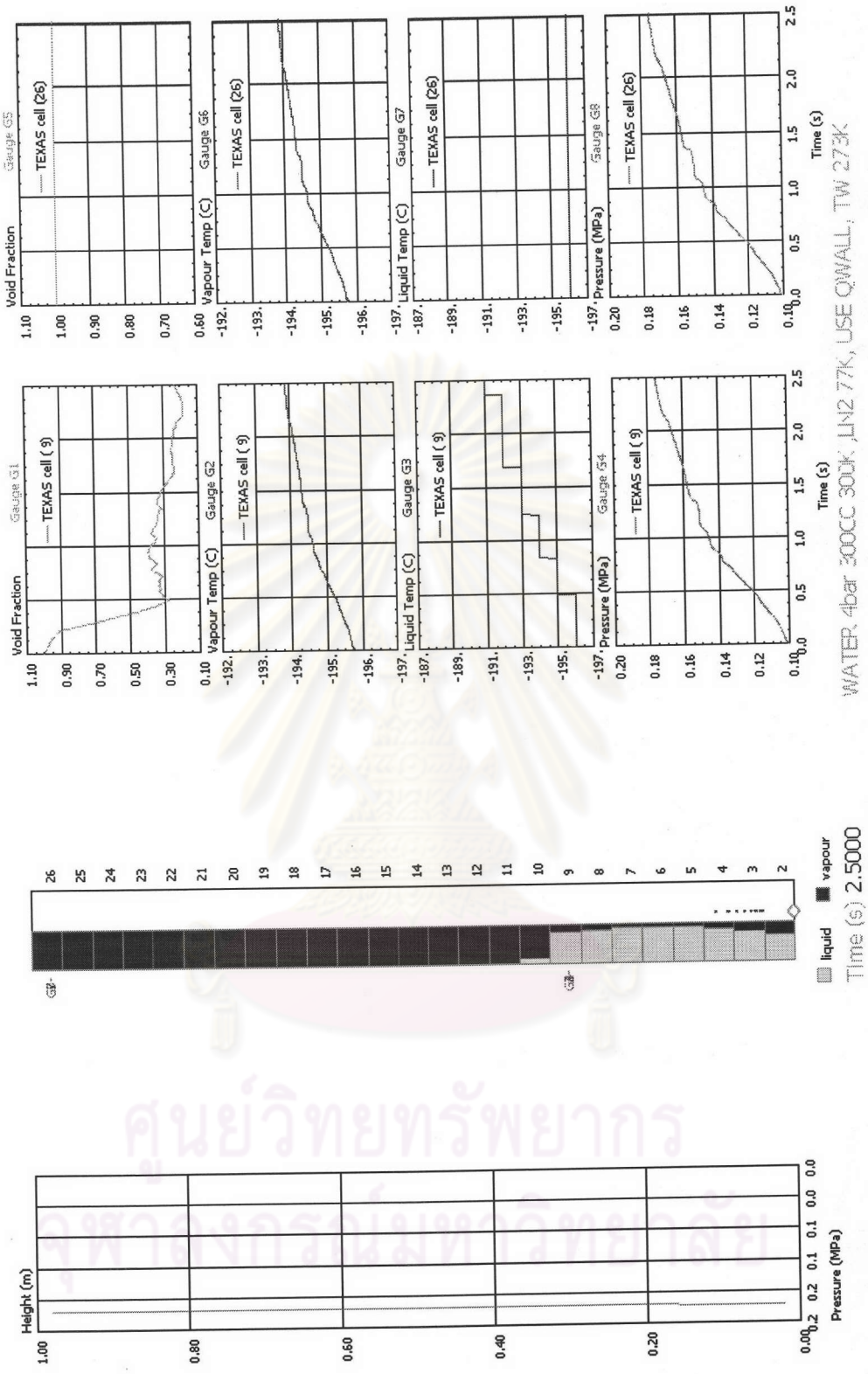

Fig. 5.13 Simulate the experiment with test conditions: Volumetric ratio is 0.15. Water injection pressure is 4 bar. Initial water, nitrogen, and wall temperatures are 300 K, 77.244 K, and 273 K, respectively. G1, G2, G3, and G4 measure the properties in Cell 9 while G5, G6, G7, and G8 measure the properties in Cell 26.

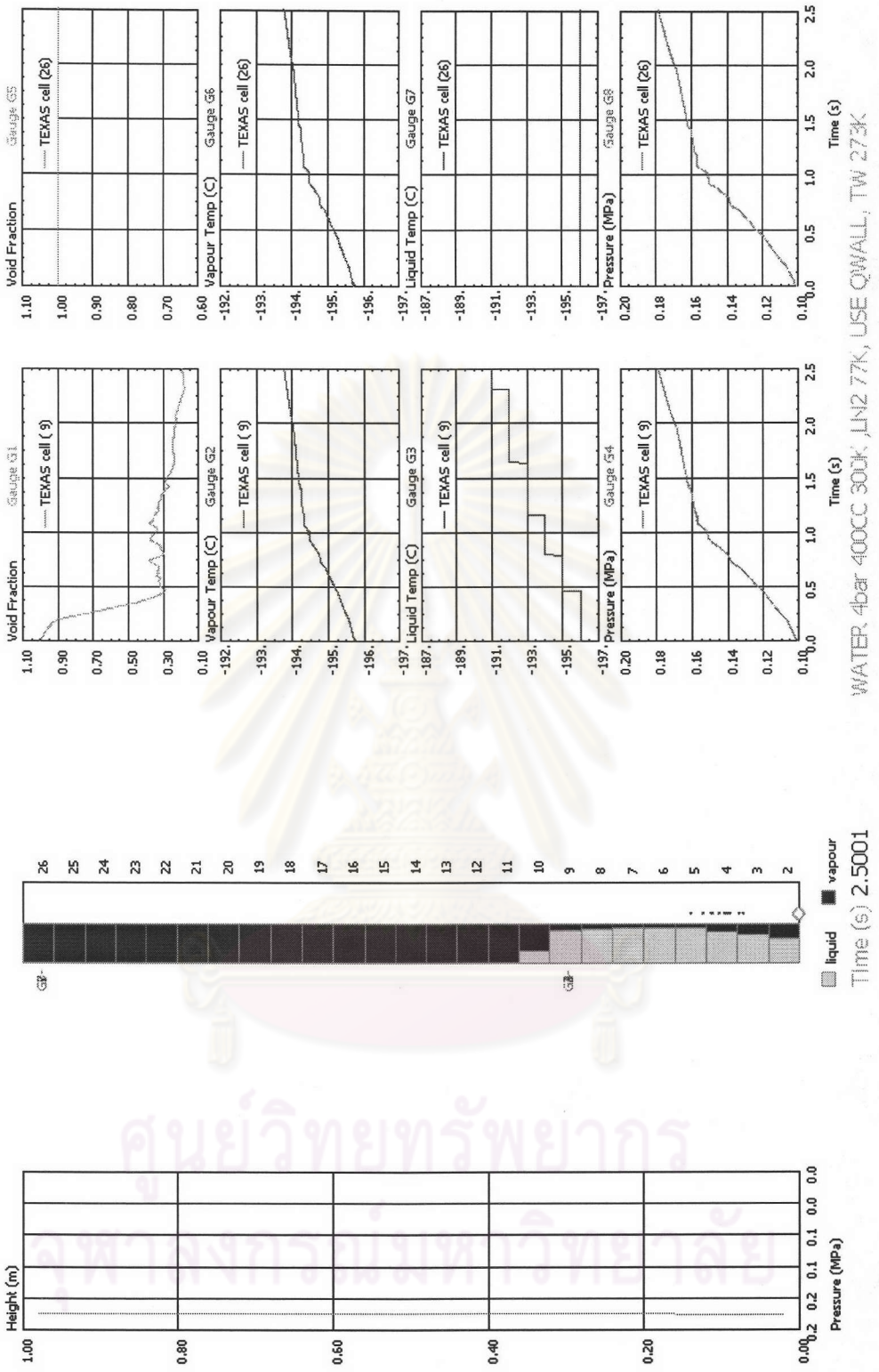

Fig. 5.14 Simulate the experiment with test conditions: Volumetric ratio is 0.20. Water injection pressure is 4 bar. Initial water, nitrogen, and wall temperatures are 300 K, 77.244 K, and 273 K, respectively. G1, G2, G3, and G4 measure the properties in Cell 9 while G5, G6, G7, and G8 measure the properties in Cell 26.

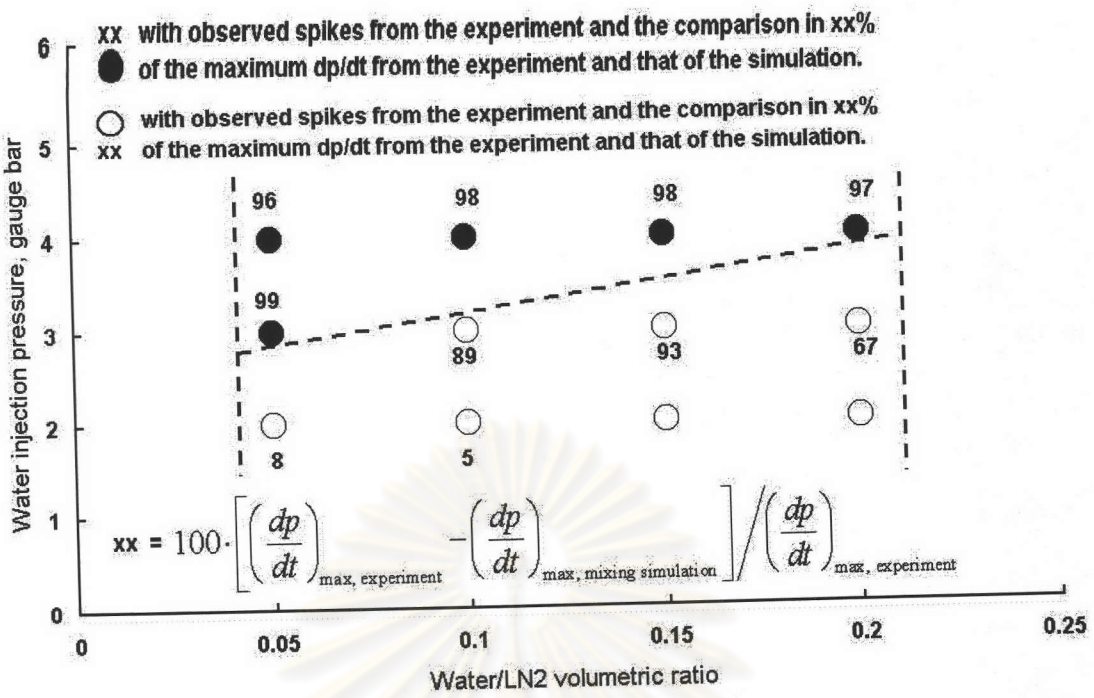

Fig. 5.15 The comparison of $\left(\frac{dp}{dt}\right)_{max}$ in percent difference from the experiment and from the simulation

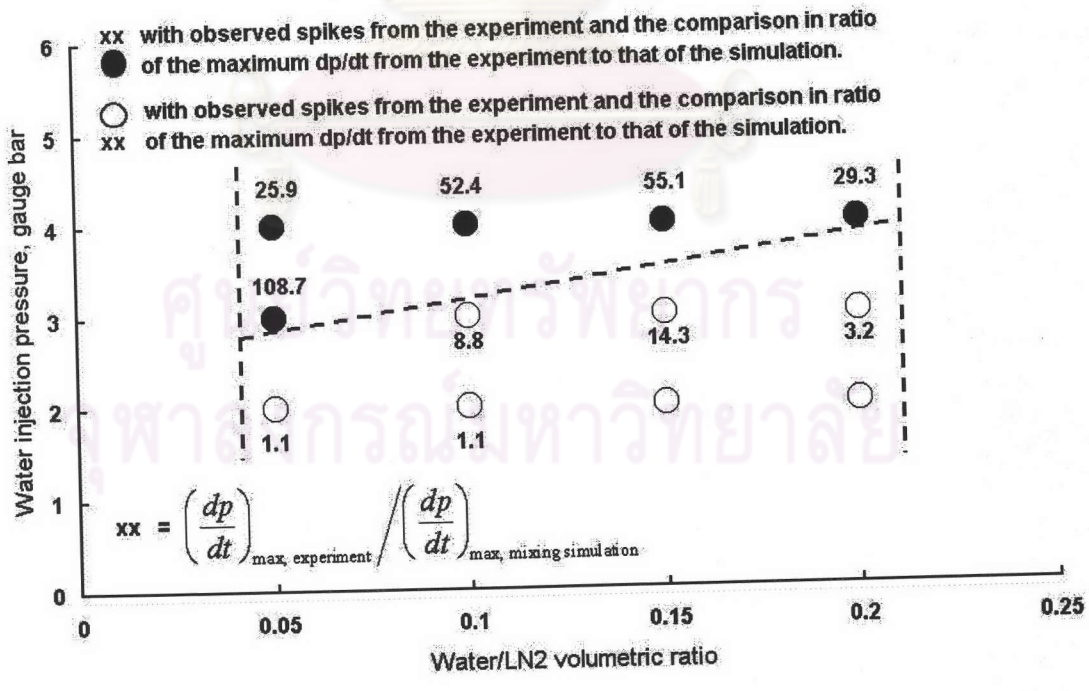

Fig. 5.16 The comparison of $\left(\frac{dp}{dt}\right)_{max}$ in ratio from the experiment and from the simulation

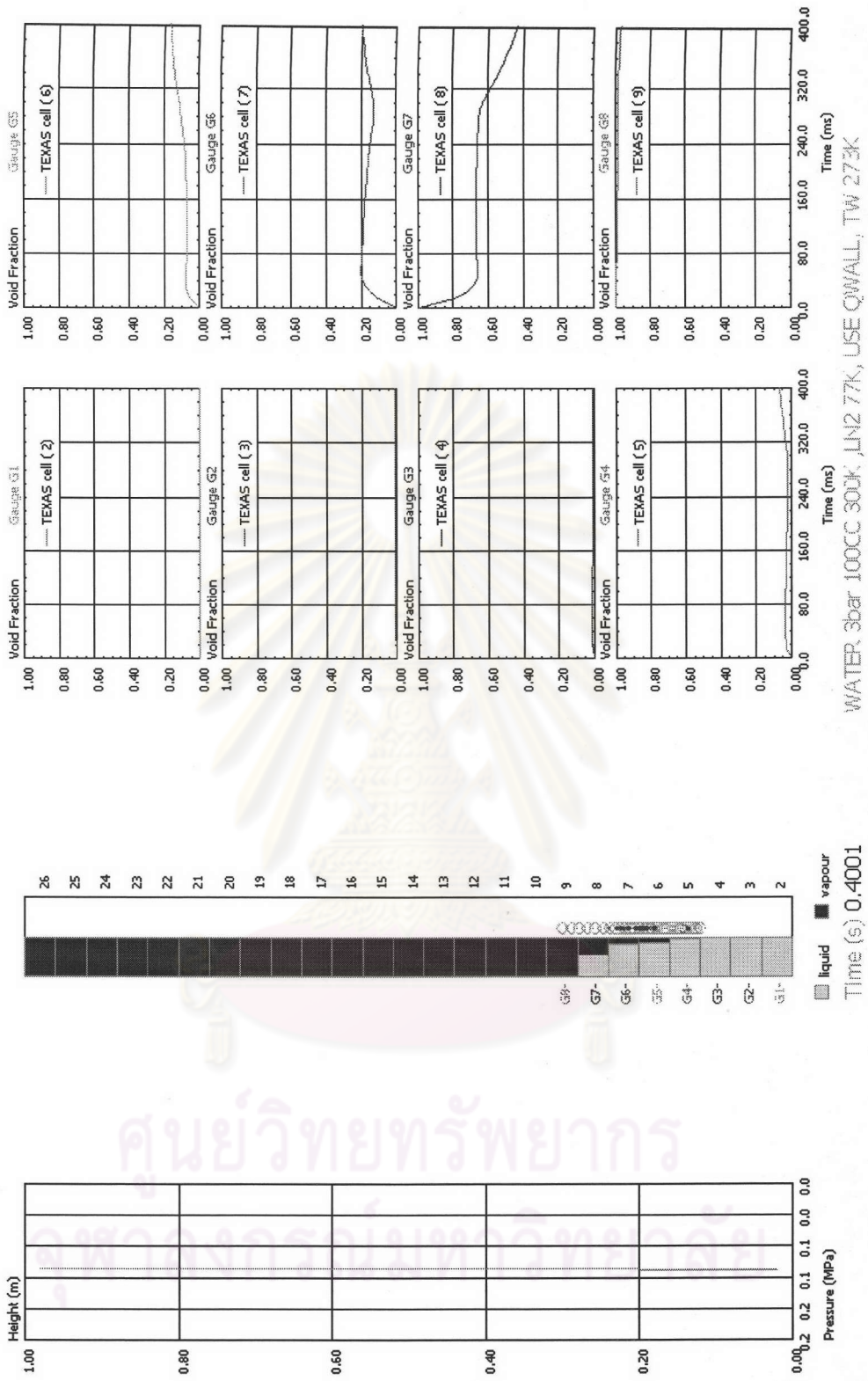

Fig. 5.17 Simulate the experiment with test conditions: Volumetric ratio is 0.05. Water injection pressure is 3 bar. Initial water, nitrogen, and wall temperatures are 300 K, 77.244 K, and 273 K, respectively. G1, G2, G3, and G4 measure the properties in Cell 9 while G5, G6, G7, and G8 measure the properties in Cell 26. The simulation stops running at the inception time.

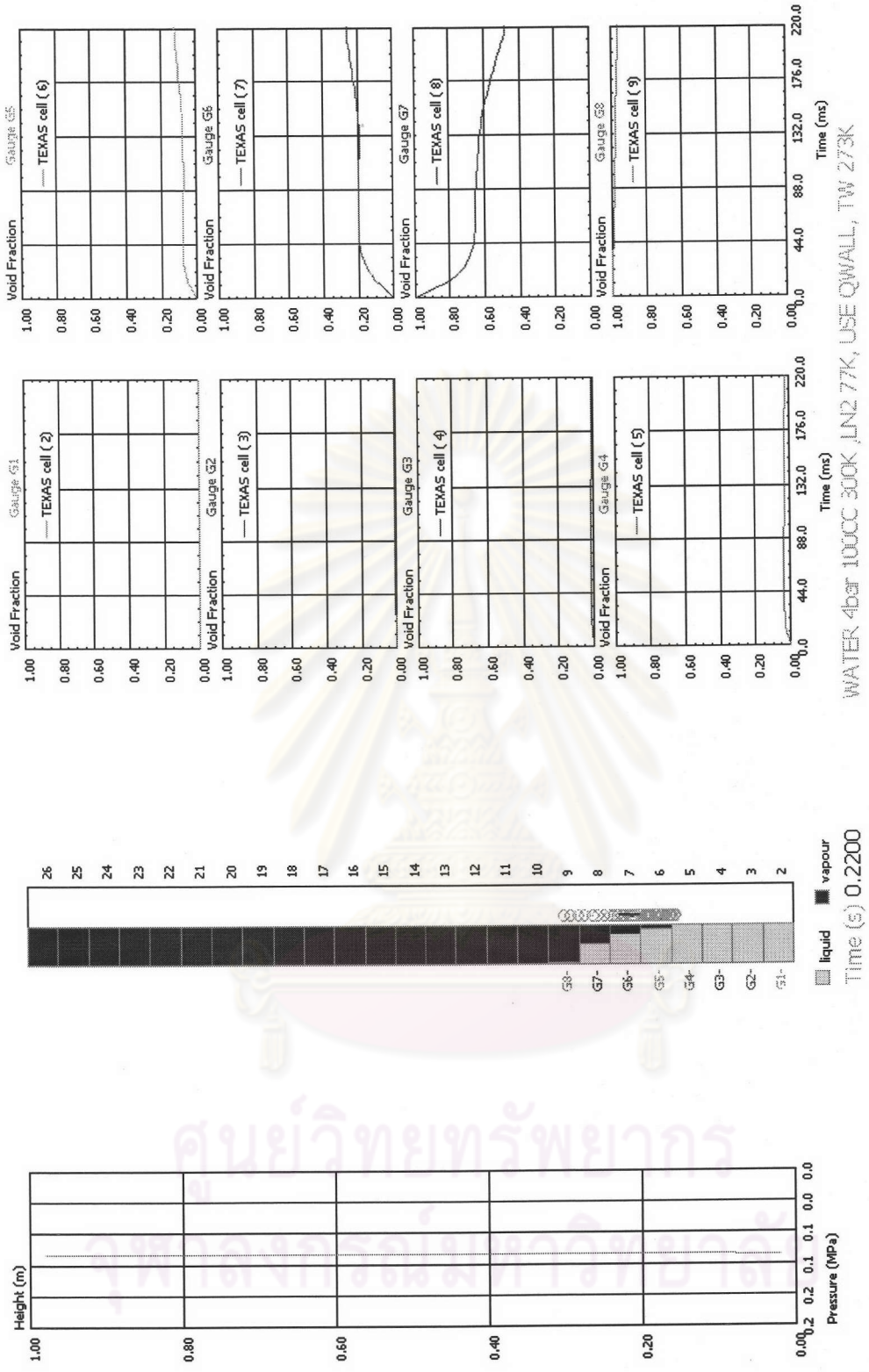

Fig. 5.18 Simulate the experiment with test conditions: Volumetric ratio is 0.05. Water injection pressure is 4 bar. Initial water, nitrogen, and wall temperatures are 300 K, 77.244 K, and 273 K, respectively. G1, G2, G3, and G4 measure the properties in Cell 9 while G5, G6, G7, and G8 measure the properties in Cell 26. The simulation stops running at the inception time.

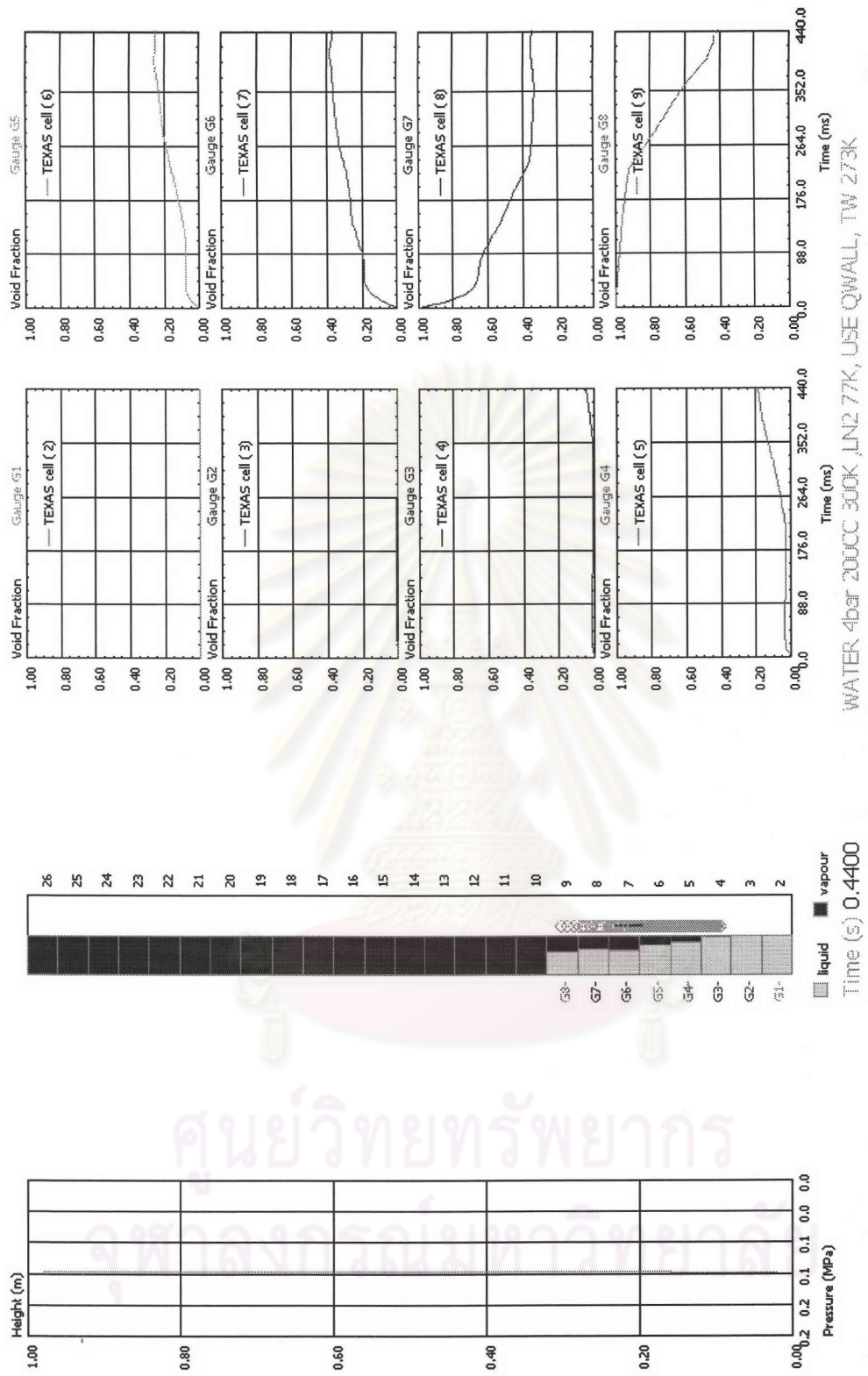

Fig. 5.19 Simulate the experiment with test conditions: Volumetric ratio is 0.10. Water injection pressure is 4 bar. Initial water, nitrogen, and wall temperatures are 300 K, 77.244 K, and 273 K, respectively. G1, G2, G3, and G4 measure the properties in Cell 9 while G5, G6, G7, and G8 measure the properties in Cell 26. The simulation stops running at the inception time.

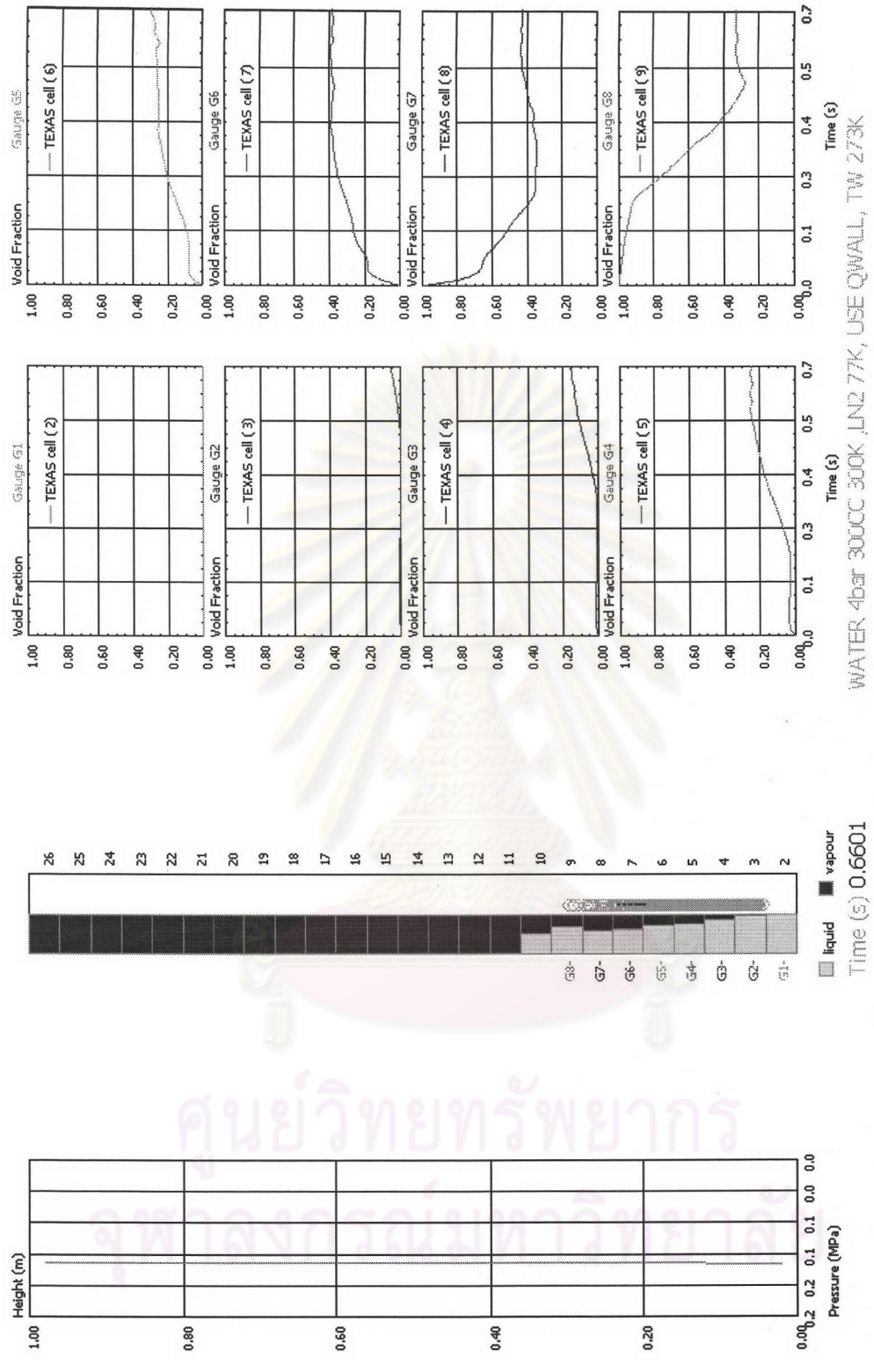

Fig. 5.20 Simulate the experiment with test conditions: Volumetric ratio is 0.15. Water injection pressure is 4 bar. Initial water, nitrogen, and wall temperatures are 300 K, 77.244 K, and 273 K, respectively. G1, G2, G3, and G4 measure the properties in Cell 9 while G5, G6, G7, and G8 measure the properties in Cell 26. The simulation stops running at the inception time.

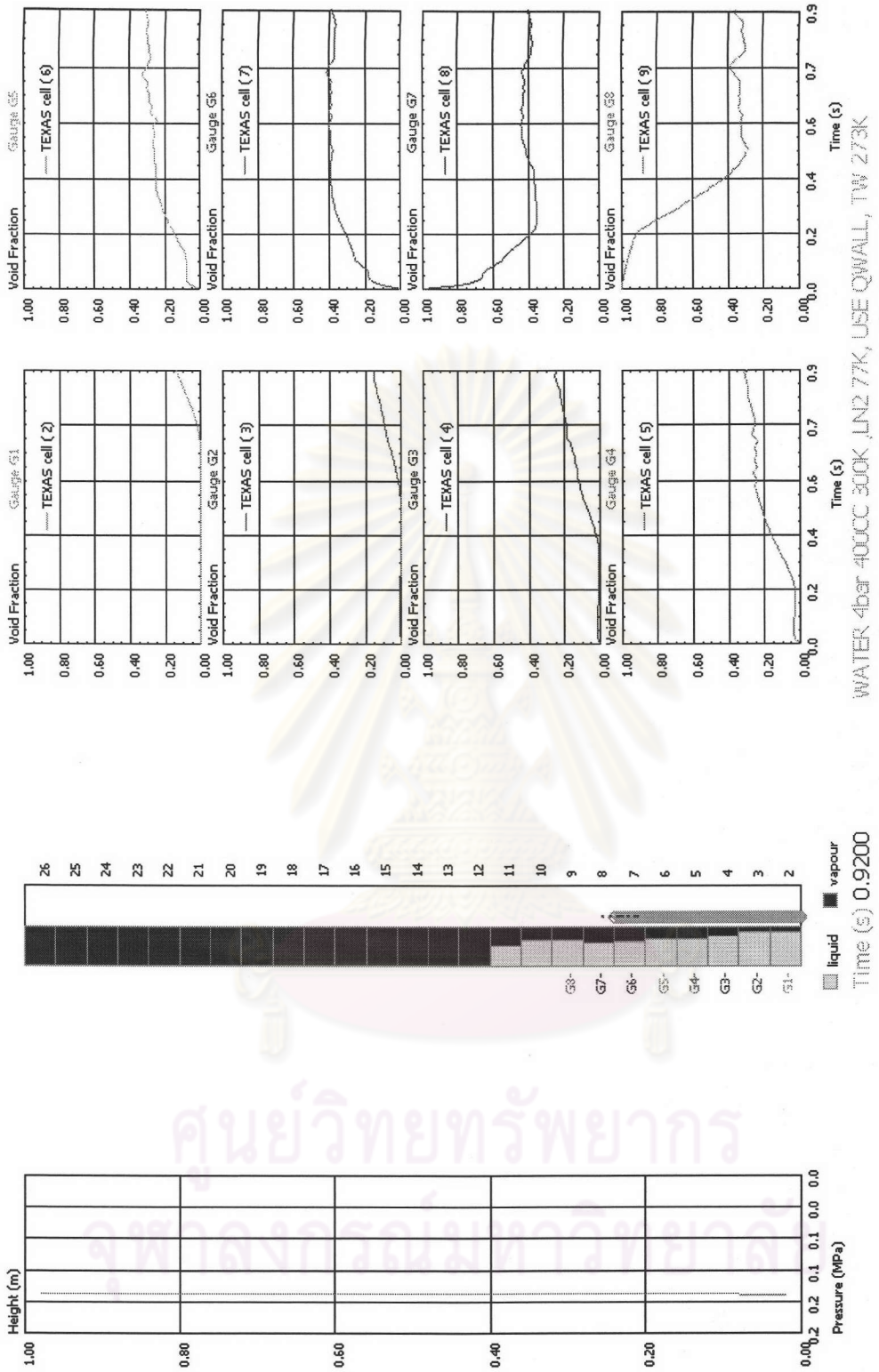

Fig. 5.21 Simulate the experiment with test conditions: Volumetric ratio is 0.20. Water injection pressure is 4 bar. Initial water, nitrogen, and wall temperatures are 300 K, 77.244 K, and 273 K, respectively. G1, G2, G3, and G4 measure the properties in Cell 9 while G5, G6, G7, and G8 measure the properties in Cell 26. The simulation stops running at the inception time.

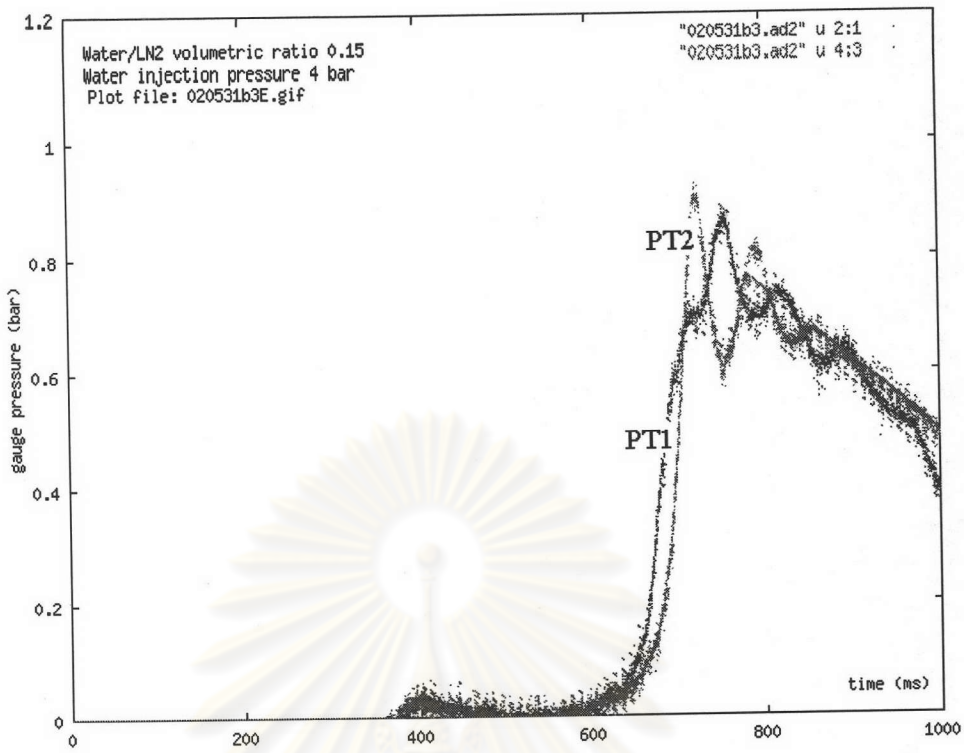

(a)

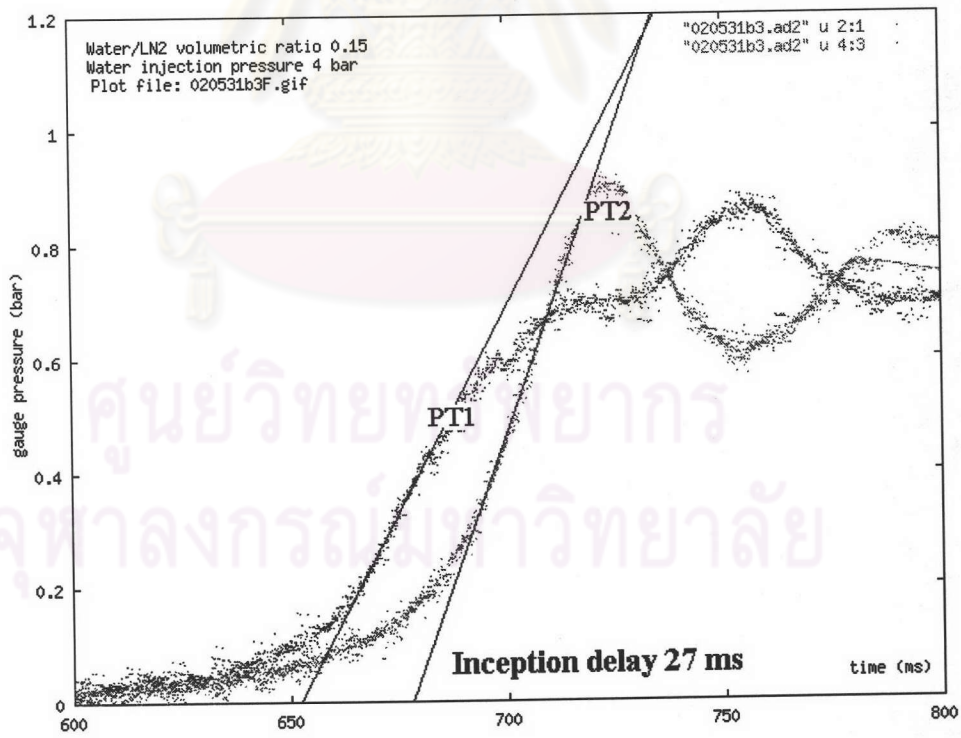

(b)

Fig. 5.22 Pressure profile after subtracting the wall heating and the mixing with the test conditions: Volumetric ratio is 0.15. Water injection pressure is 4 bar. (a) from 0-1000 ms (b) enlarged time from 600-800 ms.